ACTA ASTRONOMICA
Vol. **68** (2018) pp. 1–42

OGLE-2017-BLG-1434Lb: Eighth $q < 1 \times 10^{-4}$ Mass-Ratio Microlens Planet Confirms Turnover in Planet Mass-Ratio Function

A. Udalski[1], Y.-H. Ryu[2], S. Sajadian[3], A. Gould[2,4,5]
and
P. Mróz[1], R. Poleski[1,5], M.K. Szymański[1], J. Skowron[1],
I. Soszyński[1], S. Kozłowski[1], P. Pietrukowicz[1], K. Ulaczyk[1],
M. Pawlak[1], K. Rybicki[1], P. Iwanek[1]
(OGLE Collaboration)
M.D. Albrow[6], S.-J. Chung[2,7], C. Han[8], K.-H. Hwang[2],
Y.K. Jung[9], I.-G. Shin[9], Y. Shvartzvald[10,35], J.C. Yee[9],
W. Zang[11,12], W. Zhu[13], S.-M. Cha[2,14], D.-J. Kim[2], H.-W. Kim[2],
S.-L. Kim[2,7], C.-U. Lee[2,7], D.-J. Lee[2],
Y. Lee[2,14], B.-G. Park[2,7], R.W. Pogge[5]
(KMTNet Collaboration)
V. Bozza[15,16], M. Dominik[17], C. Helling[17], M. Hundertmark[18],
U.G. Jørgensen[19], P. Longa-Peña[20], S. Lowry[21],
M. Burgdorf[22], J. Campbell-White[21], S. Ciceri[23], D. Evans[24],
R. Figuera Jaimes[17], Y.I. Fujii[19,25], L.K. Haikala[26],
T. Henning[4], T.C. Hinse[2], L. Mancini[4,27,28], N. Peixinho[20,29],
S. Rahvar[30], M. Rabus[31,7], J. Skottfelt[32], C. Snodgrass[33],
J. Southworth[24], C. von Essen[34]
(MiNDSTEp Collaboration)

[1] Warsaw University Observatory, Al. Ujazdowskie 4, 00-478 Warszawa, Poland
email: udalski@astrouw.edu.pl
[2] Korea Astronomy and Space Science Institute, Daejon 34055, Korea
[3] Department of Physics, Isfahan University of Technology, Isfahan 84156-83111, Iran
[4] Max-Planck-Institute for Astronomy, Königstuhl 17, 69117 Heidelberg, Germany
[5] Department of Astronomy, Ohio State University, 140 W. 18th Ave., Columbus, OH 43210, USA
[6] University of Canterbury, Department of Physics and Astronomy, Private Bag 4800, Christchurch 8020, New Zealand
[7] Korea University of Science and Technology, Daejeon 34113, Korea
[8] Department of Physics, Chungbuk National University, Cheongju 28644, Republic of Korea
[9] Harvard-Smithsonian CfA, 60 Garden St., Cambridge, MA 02138, USA
[10] Jet Propulsion Laboratory, California Institute of Technology, 4800 Oak Grove Drive, Pasadena, CA 91109, USA
[11] Physics Department and Tsinghua Centre for Astrophysics, Tsinghua University, Beijing 100084, China

[12] Department of Physics, Zhejiang University, Hangzhou, 310058, China
[13] Canadian Institute for Theoretical Astrophysics, University of Toronto, 60 St George Street, Toronto, ON M5S 3H8, Canada
[14] School of Space Research, Kyung Hee University, Yongin, Kyeonggi 17104, Korea
[15] Dipartimento di Fisica "E.R. Caianiello", Università di Salerno, Via Giovanni Paolo II 132, 84084, Fisciano, Italy
[16] Istituto Nazionale di Fisica Nucleare, Sezione di Napoli, Napoli, Italy
[17] Centre for Exoplanet Science, SUPA, School of Physics & Astronomy, University of St Andrews, North Haugh, St Andrews KY16 9SS, UK
[18] Astronomisches Rechen-Institut, Zentrum für Astronomie der Universität Heidelberg (ZAH), 69120 Heidelberg, Germany
[19] Niels Bohr Institute & Centre for Star and Planet Formation, University of Copenhagen, Øster Voldgade 5, 1350 Copenhagen, Denmark
[20] Unidad de Astronomía, Universidad de Antofagasta, Av. Angamos 601, Antofagasta, Chile
[21] Centre for Astrophysics & Planetary Science, The University of Kent, Canterbury CT2 7NH, UK
[22] Universität Hamburg, Faculty of Mathematics, Informatics and Natural Sciences, Department of Earth Sciences, Meteorological Institute, Bundesstraße 55, 20146 Hamburg, Germany
[23] Department of Astronomy, Stockholm University, Alba Nova University Center, 106 91, Stockholm, Sweden
[24] Astrophysics Group, Keele University, Staffordshire, ST5 5BG, UK
[25] Institute for Advanced Research, Nagoya University, Furo-cho, Chikusa-ku, Nagoya, 464-8601, Japan
[26] Instituto de Astronomia y Ciencias Planetarias de Atacama, Universidad de Atacama, Copayapu 485, Copiapo, Chile
[27] Department of Physics, University of Rome Tor Vergata, Via della Ricerca Scientifica 1, I-00133-Roma, Italy
[28] INAF – Astrophysical Observatory of Turin, Via Osservatorio 20, I-10025 – Pino Torinese, Italy
[29] CITEUC – Center for Earth and Space Research of the University of Coimbra, Geophysical and Astronomical Observatory, R. Observatorio s/n, 3040-004 Coimbra, Portugal
[30] Department of Physics, Sharif University of Technology, PO Box 11155-9161 Tehran, Iran
[31] Instituto de Astrofísica, Pontificia Universidad Católica de Chile, Av. Vicuña Mackenna 4860, 7820436 Macul, Santiago, Chile
[32] Centre for Electronic Imaging, Department of Physical Sciences, The Open University, Milton Keynes, MK7 6AA, UK
[33] School of Physical Sciences, Faculty of Science, Technology, Engineering and Mathematics, The Open University, Walton Hall, Milton Keynes, MK7 6AA, UK
[34] Stellar Astrophysics Centre, Department of Physics and Astronomy, Aarhus University, Ny Munkegade 120, 8000 Aarhus C, Denmark
[35] NASA Postdoctoral Program Fellow

Received February 8, 2018

ABSTRACT

We report the discovery of a cold Super-Earth planet ($m_p = 4.4 \pm 0.5$ M$_\oplus$) orbiting a low-mass ($M = 0.23 \pm 0.03$ M$_\odot$) M dwarf at projected separation $a_\perp = 1.18 \pm 0.10$ a.u., *i.e.*, about 1.9 times the distance the snow line. The system is quite nearby for a microlensing planet, $D_L = 0.86 \pm 0.09$ kpc. Indeed, it was the large lens-source relative parallax $\pi_{\rm rel} = 1.0$ mas (combined with the low mass M) that gave rise to the large, and thus well-measured, "microlens parallax" $\pi_{\rm E} \propto (\pi_{\rm rel}/M)^{1/2}$ that enabled these precise measurements. OGLE-2017-BLG-1434Lb is the eighth microlensing planet with planet-host mass ratio $q < 1 \times 10^{-4}$.

We apply a new planet-detection sensitivity method, which is a variant of "$V/V_{\rm max}$", to seven of these eight planets to derive the mass-ratio function in this regime. We find $\mathrm{d}N/\mathrm{d}\ln q \propto q^p$, with $p = 1.05^{+0.78}_{-0.68}$, which confirms the "turnover" in the mass function found by Suzuki *et al.* relative to the power law of opposite sign $n = -0.93 \pm 0.13$ at higher mass ratios $q \gtrsim 2 \times 10^{-4}$. We combine our result with that of Suzuki *et al.* to obtain $p = 0.73^{+0.42}_{-0.34}$.

Key words: *Gravitational lensing: micro – Planetary systems*

1. Introduction

Microlensing searches are finding planets with planet/host mass ratio q that are nearly uniformly distributed in $\log q$ over $-4.3 \lesssim \log q \lesssim -2$ (Figs. 7 and 8 of Mróz *et al.* 2017). Since planet detectability grows with q, this immediately implies a steeply rising mass function toward lower mass ratios. In the first study to measure this relation, Sumi *et al.* (2010) found $\mathrm{d}N/\mathrm{d}\log q \propto q^n$ with $n = -0.7 \pm 0.2$. Naively, the almost perfectly flat distribution cataloged by Mróz *et al.* (2017) over a 2.3 dex range in q would indeed appear to argue for a single power law. However, Suzuki *et al.* (2016) subsequently argued for a break in the power law at about $\log q \approx -3.75$, with $n = -0.93 \pm 0.13$ above the break. Below the break they found a sign reversal in the power law, $\mathrm{d}N/\mathrm{d}\log q \propto q^p$ with $p = 0.6^{+0.5}_{-0.4}$, implying a true "turnover" at the break. The main argument for this break is that existing planet surveys had significant sensitivity to planets below the break, but found very few. In particular, the Microlensing Observations in Astrophysics (MOA) survey, which was the primary data set that they analyzed, had only two planets with $\log q < -4$ (or four in extended sample). Note, however, that another recent study by Shvartzvald *et al.* (2016), based on the overlap of the OGLE, MOA and Wise surveys, fit to a single power law and found $n = -0.50 \pm 0.17$.

A confirmation and refined measurement (or, alternatively, refutation) of the Suzuki *et al.* (2016) break and turnover would be of great interest to constrain theories of planetary formation. Moreover, it would also be of immediate practical interest in devising strategies for WFIRST microlensing observations (Spergel *et al.* 2013). Since WFIRST will be far more sensitive to planets below the Suzuki *et al.* (2016) break than ground-based surveys, its planet discovery rate is much more sensitive to such a break.

Here, we report the discovery of the low mass ratio $q = 5.8 \times 10^{-5}$ planet OGLE-2017-BLG-1434Lb. This is the eighth microlensing planet with a mass ratio that is securely in the range $\log q < -4$, meaning that the sample that lies clearly

below the Suzuki *et al.* (2016) break is now large enough for robust statistical investigation. On the other hand, in contrast to the Suzuki *et al.* (2016) sample, these eight planets are drawn from quite heterogeneous detection processes. Therefore proper statistical analysis requires great care.

There are two other notable features of the discovery of OGLE-2017-BLG-1434Lb. First, we are able to make an accurate mass measurement, thanks to a clear detection of the microlens parallax parameter,

$$\boldsymbol{\pi}_{\rm E} \equiv \pi_{\rm E} \frac{\boldsymbol{\mu}_{\rm rel}}{\mu_{\rm rel}}, \qquad \pi_{\rm E} \equiv \frac{\pi_{\rm rel}}{\theta_{\rm E}} \tag{1}$$

where $\pi_{\rm rel} \equiv {\rm a.u.}(D_L^{-1} - D_S^{-1})$ and $\boldsymbol{\mu}_{\rm rel}$ are the lens-source relative parallax and proper motion, respectively,

$$\theta_{\rm E} \equiv \sqrt{\kappa M \pi_{\rm rel}}, \qquad \kappa \equiv \frac{4G}{c^2 {\rm a.u.}} \simeq 8.14 \frac{\rm mas}{{\rm M}_\odot}, \tag{2}$$

and M is the lens mass. Note that when $\pi_{\rm E}$ and $\theta_{\rm E}$ are both measured, $M = \theta_{\rm E}/\kappa\pi_{\rm E}$ can likewise be determined (Gould 1992, 2000, 2004, Gould and Horne 2013)

Of the eight planets with $\log q < -4$, five have good-to-excellent mass measurements, which is a remarkably high fraction. Two of these (including OGLE-2017-BLG-1434) have excellent ground-based parallax measurements, one has a good ground-based parallax measurement, one has an excellent space-based parallax measurement using Spitzer satellite, and for the last, the host was directly imaged 8.2 years after the event. This high rate of mass measurements permits at least a qualitative statement about the distribution of host masses of low mass-ratio planets.

Second, although OGLE-2017-BLG-1434 is within a factor 1.3 of the lowest mass-ratio microlensing planet, we show that it would have been both detected and well-characterized even if it were a factor 30 smaller in q, *i.e.*, $\log q = -5.71$, or approximately 12 Moon masses. This demonstrates that microlensing studies, at least in their current configuration, can probe to substantially smaller masses than have yet been reported as discoveries, and hence further motivates an investigation of whether there is really a break in the mass-ratio function near $\log q \approx -4$.

2. Observations

OGLE-2017-BLG-1434 is at (RA,Dec)$_{\rm J2000}$ = (17:53:07.29, −30:14:44.6), corresponding to $(l,b) = (-0.28, -2.07)$. It was discovered and announced as a probable microlensing event by the OGLE Early Warning System (Udalski *et al.* 1994, Udalski 2003) at UT 19:33 July 25, 2017[1]. The event lies in OGLE field

[1]The same microlensing event triggered an alert (OGLE-2017-BLG-1392) on a different catalog star 1.″08 from OGLE-2017-BLG-1434 at UT 19:14 20 Jul, *i.e.*, 5.0 d earlier. We find that the source star lies at $({\rm RA}, {\rm Dec}) = (17{:}53{:}07.25,\ -30{:}14{:}44.5)$, which is roughly half way between these two catalog stars, but slightly closer to OGLE-2017-BLG-1434.

BLG501 (Udalski *et al.* 2015), for which OGLE observations were at a cadence of $\Gamma = 1$ hr^{-1} during the 2017 season using their 1.3 m Warsaw telescope at Las Campanas, Chile.

The Korea Microlensing Telescope Network (KMTNet, Kim *et al.* 2016) observed this field from its three 1.6 m telescopes at CTIO (Chile, KMTC), SAAO (South Africa, KMTS) and SSO (Australia, KMTA), in its two slightly offset fields BLG01 and BLG41, with combined cadence of $\Gamma = 4$ hr^{-1} .

The great majority of these survey observations were carried out in *I*-band with occasional *V*-band observations made solely to determine source colors. All reductions for the light curve analysis were conducted using variants of difference image analysis (DIA, Alard and Lupton 1998), specifically Woźniak (2000) and Albrow *et al.* (2009).

The MiNDSTEp collaboration observed OGLE-2017-BLG-1434 from the 1.54 m Danish Telescope at La Silla, Chile, using an EMCCD camera operated at 10 Hz and with a broad passband approximating the *I*-band filter, with mean response at 770 nm (Skottfelt *et al.* 2015, Evans *et al.* 2016). The data were reduced using an updated version of the DanDIA pipeline (Bramich 2008). These observations were initiated with 10 exposures on the night of $\mathrm{HJD}' \equiv \mathrm{HJD} - 2\,450\,000 = 7981$ and continually increased to 75 exposures on $\mathrm{HJD}' = 7984$, *i.e.*, the night closest to the predicted peak, falling to 50 exposures the following night. Based on these last observations, MiNDSTEp issued an alert, triggered by SIGNALMEN (Dominik *et al.* 2007), of a possible anomaly, which it confirmed the next day based on OGLE online data. MiNDSTEp then continued regular observations of the event until the night of $\mathrm{HJD}' = 7998$.

3. Analysis

With the exception of some deviations near the peak that last slightly more than one day, the overall shape of the OGLE-2017-BLG-1434 light curve (Fig. 1) is that of an ordinary point-lens (Paczyński 1986) event. Excluding the deviation, the change in magnitude from baseline to peak (≈ 2.5 mag) implies a magnification $A \gtrsim 10$ (higher if there is significant blending). The two most obvious components of the deviation are a flat trough that lies about 0.7 mag below the level of the point-lens curve and lasts 0.4 d (traced in KMTS, OGLE, KMTC, and MiNDSTEp data), followed by a very rapid caustic entrance (traced in KMTC, OGLE, and MiNDSTEp data). Once these features are noted, it becomes clear that the underlying light curve is essentially symmetric and that the onset of a caustic exit is traced by KMTA data just before the trough.

This trough is an unambiguous signature of a "minor image perturbation". The point-lens light curve (due to the host in the absence of a companion) is generated by two images of the source. The major image forms at a minimum in the time-delay surface (in accord with Fermat's principle), while the minor image forms at a saddle point. The latter is highly unstable, so that if a small planet lies at or near the position of this image, the image will be virtually annihilated. The flux ratio of the

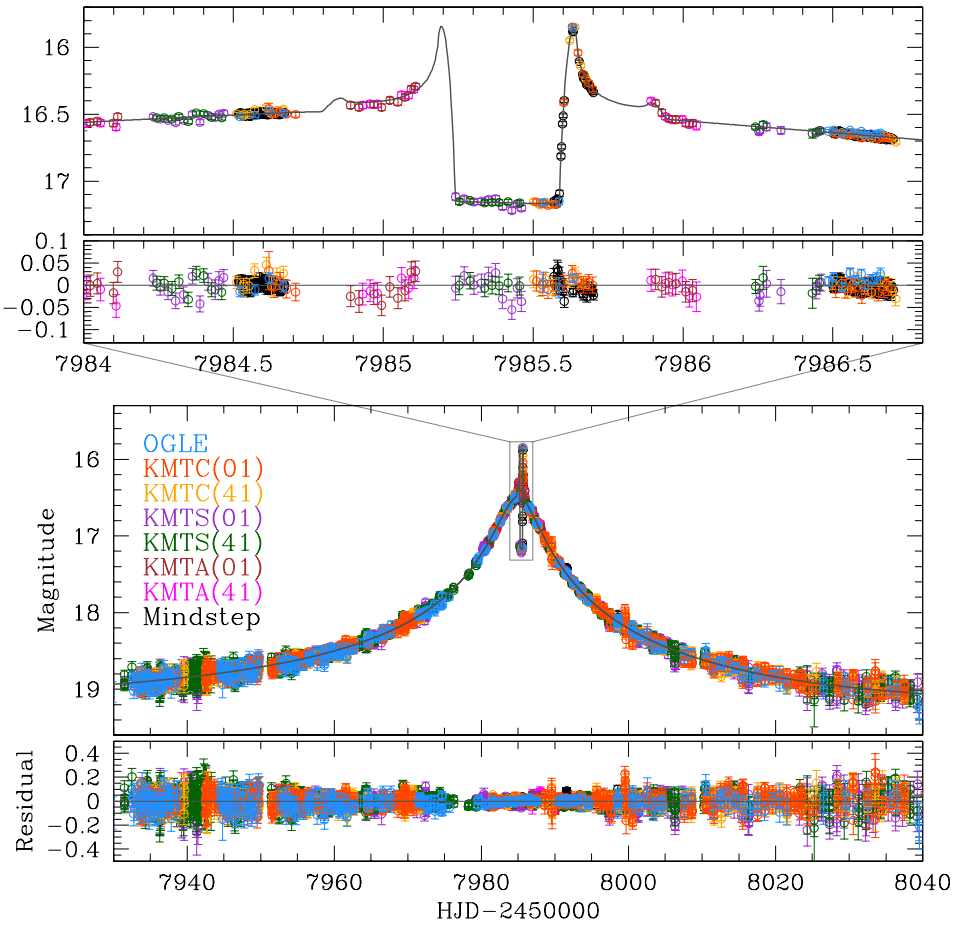

Fig. 1. Light curve and best-fit model of OGLE-2017-BLG-1434. As discussed in Section 3, many of the key parameters can be "read off" the light curve, including that this is a very low mass-ratio planet: $q < 10^{-4}$. Data are color-coded by observatory.

two images is $\eta = (A-1)/(A+1)$ where A is the total magnification. Hence, for a high-magnification event such as this one, $\eta \to 1$, which means that annihilating the minor image should decrease the total flux by half, *i.e.*, ≈ 0.75 mag. That is, the light curve's behavior exactly corresponds to this expectation.

Such troughs are always aligned with the planet-star axis and are flanked by two caustics. However, the troughs generally extend substantially beyond the caustics. Hence, if the source trajectory crosses the trough at a point where there are no caustics, its entrance and exit to the trough will be smooth. However, if it crosses the caustics, the trough entrance and exit will correspond to a sharp (discontinuous slope) caustic exit and entrance, respectively. The latter is clearly the geometry of OGLE-2017-BLG-1434.

Of course, after exiting the trough (so, entering the caustic), the source must again exit the caustic. Because the caustic edge facing the trough is much stronger

than its "outer walls", the effect on the light curve is much less pronounced. Nevertheless, this outer-edge crossing was captured in the first three KMTA points after the trough.

If the trough occurs at relatively low magnification, then each of the two caustic "walls" that flank the caustic will be part of triangular caustic structures. However, at progressively higher magnification (corresponding to planets that are progressively closer to the Einstein ring), these triangular caustics grow in size and progressively move toward the quadrilateral central caustic close to the host. The triangular caustics eventually merge with the central caustic to form a single, six-sided caustic (Fig. 4 of Gaudi 2012). This turns out to be the geometry of OGLE-2017-BLG-1434. See Fig. 2.

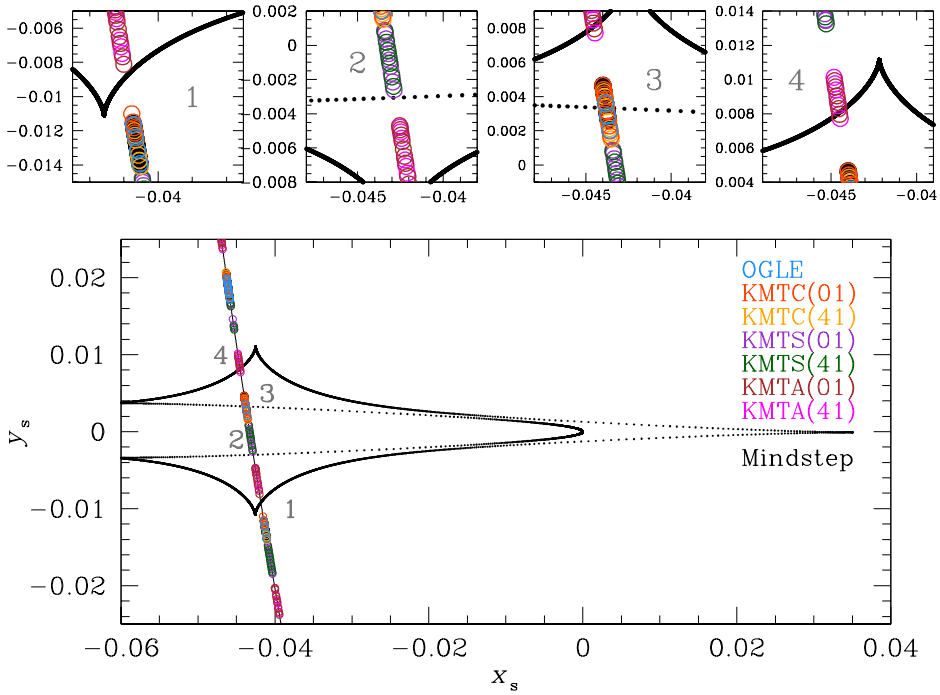

Fig. 2. Caustic diagram of OGLE-2017-BLG-1434. The source passes over the "planetary wing" of a resonant caustic, resulting from the planet perturbing the minor image. The points are color coded by observatory, and their size represents the scaled source $\rho = 4.5 \times 10^{-4}$ of the best fit model.

Continuing this logic, one can approximately read off the parameters of a standard seven-parameter model from the light curve, using known analytic formula (Han 2006) for the caustics. Three of these parameters (t_0, u_0, t_E) correspond to the time of maximum, impact parameter, and Einstein crossing time of the underlying point-lens (Paczyński 1986) model. Three others (s, q, α) describe the binary companion, namely its separation (in units of θ_E), its mass ratio, and the angle of the binary axis relative to the source trajectory. Finally, if (as in the present case) the

source passes over or near the caustics, one must specify $\rho = \theta_*/\theta_E$, *i.e.*, the ratio of the source radius to the Einstein radius.

A point-lens fit to the light curve with the anomaly removed yields $(t_0, u_0, t_E) = (7984.94, 0.027, 95\,\mathrm{d})$, which implies an effective timescale $t_{\rm eff} \equiv u_0 t_E = 2.57$ d. The anomaly is centered $\delta t = 0.5$ d after peak, implying that $\alpha = \mathrm{atan}(-t_{\rm eff}/\delta t) = \pm 259^\circ$ and that s should satisfy, $s^{-1} - s = u_0\sqrt{1+(\delta t/t_{\rm eff})^2}$, which implies[2] $s \simeq 1 - u_0/2 = 0.986$. From the light curve, the duration of the trough is $\Delta t \simeq 0.4$ d. (It could in principle be slightly larger because the caustic exit is not actually observed. However, the rise toward the caustic is observed from KMTA, so this estimate cannot be far off.) This quantity can be related to the Han (2006) parameter $\eta_{c-} = 2q^{1/2}(s^{-2}-1)^{1/2}$ by $\Delta t = 2t_E\eta_{c-}|\sec\alpha|$, which for the present case implies $q \simeq u_0(\Delta t/t_{\rm eff})^2/16 = 4.1\times10^{-5}$. Finally, the rise time of the caustic exit in OGLE/KMTC/MiNDSTEp data is $t_{\rm rise} = 66$ min. From Gould and Andronov (1999), $t_{\rm rise} = 1.7 t_* \sec\alpha$, where $t_* = \rho t_E$. Hence, $t_* = 39$ min and $\rho \simeq (t_*/t_E) = 3.5\times10^{-4}$.

However, following from these results, it is obvious that additional higher order effects should be measurable. First note that ρ is unusually small, so that the Einstein radius $\theta_E = \theta_*/\rho \simeq 3000\,\theta_*$. We will estimate the source size θ_* in detail in Section 4.1. However, just from the source flux derived from the Paczyński (1986) fit, it is an upper main sequence star, *i.e.*, $\theta_* \sim 0.5\,\mu$as.

Such a large Einstein radius ($\theta_E \approx 1.5\,\mu$as) immediately implies that the host must be either a dark remnant (black hole or neutron star) or it must be quite nearby. That is, from the definition of θ_E (Eq. 2),

$$\pi_{\rm rel} = \frac{\theta_E^2}{\kappa M} \rightarrow 0.3\,\mu{\rm as}\left(\frac{M}{M_\odot}\right)^{-1}. \tag{3}$$

Indeed, since a solar-mass star at $D_L \approx 2.5$ kpc would easily be visible, the actual lens must have even lower mass (hence higher $\pi_{\rm rel}$). Therefore, again unless the host is a dark remnant, the microlens parallax must be fairly large.

$$\pi_E = \frac{\pi_{\rm rel}}{\theta_E} > 0.2. \tag{4}$$

Given that the event is quite long, such a parallax should be measurable.

Thus, without any detailed modeling, one can infer that there should be a strong microlens parallax signal and that the implications of not finding such a signal would be striking.

When introducing the two parallax parameters $\boldsymbol{\pi}_E = (\pi_{E,N}, \pi_{E,E})$, one must also, at least initially, introduce linearized orbital motion parameters $({\rm d}s/{\rm d}t, {\rm d}\alpha/{\rm d}t)$ as well. These encode the instantaneous rate of change in the separation and orientation of the binary at t_0. There are two reasons that these must be included. First, the orbital motion parameters $({\rm d}s/{\rm d}t, {\rm d}\alpha/{\rm d}t)$ can be correlated with $\boldsymbol{\pi}_E$, so

[2]The other $(s > 1)$ solution is excluded because it would correspond to the major image.

that by ignoring them one can induce artificial effects in the parallax (Skowron *et al.* 2011, Batista *et al.* 2011, Han *et al.* 2016). Second, binary systems are known *a priori* to orbit their center of mass. Hence, there is no viable reason for excluding these parameters except if they are better constrained by the fact that physical systems ought to be bound than they are by the data. However, while (as described above) there are very strong reasons to believe that the parallax parameters can be measured, there is no corresponding confidence with respect to $(\mathrm{d}s/\mathrm{d}t, \mathrm{d}\alpha/\mathrm{d}t)$. Therefore, these parameters must be handled carefully. See, *e.g.*, Ryu *et al.* (2017).

Notwithstanding the above analytic arguments, we conduct a grid search over (s, q, α), seeded by the above values of $(t_0, u_0, t_\mathrm{E}, \rho)$, with all parameters except (s, q) allowed to vary and apply χ^2 minimization using a Markov Chain Monte Carlo (MCMC). To evaluate the magnifications at individual data points, we use inverse ray shooting in and near the caustics (Kayser *et al.* 1986, Schneider and Weiss 1988, Wambsganss 1997) and multipole approximations (Pejcha and Heyrovský 2009, Gould 2008) elsewhere. We employ a linear limb-darkening coefficient $\Gamma_I = 0.429$ based on the source type derived in Section 4.1.

We find only one solution. This is close to the one derived above analytically in terms of (s, α) and the so-called invariant quantities (Yee *et al.* 2012, Ryu *et al.* 2017): $(s, \alpha, t_\mathrm{eff}, t_*, qt_\mathrm{E}) = [0.981, 259^\circ, (2.59, 0.0284, 0.00364)\ \mathrm{d}]$ compared to $[0.986, 259^\circ, (2.57, 0.0271, 0.00389)\ \mathrm{d}]$ "predicted". The major difference is only in t_E, which can be significantly impacted by unmodeled parallax for long timescale events.

We then introduce the higher-order parameters $\boldsymbol{\pi}_\mathrm{E} = (\pi_{\mathrm{E},N}, \pi_{\mathrm{E},E})$ and $\boldsymbol{\gamma} = ((\mathrm{d}s/\mathrm{d}t)/s,\ \mathrm{d}\alpha/\mathrm{d}t)$. We find that in a completely free fit, three of these are well constrained, but the fourth $(\gamma_\perp = \mathrm{d}\alpha/\mathrm{d}t)$ is not. In particular, we find that for most of the solution space, the (absolute value of the) ratio of projected kinetic to potential energy (Batista *et al.* 2011),

$$\beta \equiv \left(\frac{\mathrm{KE}}{\mathrm{PE}}\right)_\perp = \frac{\kappa \mathrm{M}_\odot\, \mathrm{yr}^2}{8\pi^2} \frac{\pi_\mathrm{E}}{\theta_\mathrm{E}} \frac{s^3 \gamma^2}{(\pi_\mathrm{E} + \pi_s/\theta_\mathrm{E})^3}, \tag{5}$$

violates the boundedness condition, $\beta < 1$. Here, we adopt $\pi_s = 0.117$ mas for the source parallax. We address this by making two different calculations. First, we arbitrarily set $\boldsymbol{\gamma} = 0$. Of course, as mentioned above, this is unphysical, but it is simple and is useful as a benchmark for the second calculation, in which we allow $\boldsymbol{\gamma}$ to vary but restrict $\beta < 0.7$, *i.e.*, a limit that would be satisfied by the overwhelming majority of real, bound systems[3].

The results are shown in Table 1. The first point is that the parallax+orbital models in which β is restricted to a reasonable physical range $\beta < 0.7$ yield statistically indistinguishable results from the parallax-only models in which $\beta = \gamma = 0$. That is, our inability to fully measure γ does not significantly influence the measurement of any other parameter.

[3]The results hardly differ if we choose the extreme physical limit $\beta < 1$.

Second, while there are two degenerate $(\pm u_0)$ models with similar χ^2, their parameters (apart from the sign of u_0) are the same within 1σ. Hence, this degeneracy does not materially impact the inferred physical parameters of the system.

T a b l e 1

Best-fit solutions

Parameters	Standard	Parallax models		Parallax+Orbital motion models	
		$u_0 > 0$	$u_0 < 0$	$u_0 > 0$	$u_0 < 0$
χ^2/dof	21418.644/18659	18658.511/18657	18662.277/18657	18654.143/18655	18658.155/18655
t_0 [HJD']	7984.935 ± 0.004	7984.979 ± 0.004	7984.978 ± 0.004	7984.978 ± 0.004	7984.977 ± 0.004
u_0	0.037 ± 0.001	0.044 ± 0.001	-0.044 ± 0.001	0.043 ± 0.001	-0.043 ± 0.001
$t_{\rm E}$ [d]	72.856 ± 0.907	61.421 ± 0.692	62.981 ± 0.788	62.957 ± 0.863	64.255 ± 1.006
s	0.980 ± 0.0003	0.978 ± 0.0003	0.978 ± 0.0003	0.979 ± 0.0004	0.979 ± 0.0003
q (10^{-5})	4.938 ± 0.057	5.866 ± 0.063	5.571 ± 0.077	5.722 ± 0.145	5.607 ± 0.152
α [rad]	4.535 ± 0.001	4.552 ± 0.001	-4.556 ± 0.002	4.551 ± 0.002	-4.553 ± 0.002
ρ (10^{-4})	4.019 ± 0.060	4.815 ± 0.068	4.679 ± 0.072	4.692 ± 0.093	4.643 ± 0.099
$\pi_{\rm E,N}$	–	-0.491 ± 0.079	-0.508 ± 0.083	-0.586 ± 0.081	-0.562 ± 0.081
$\pi_{\rm E,E}$	–	0.471 ± 0.013	0.475 ± 0.013	0.472 ± 0.013	0.471 ± 0.013
ds/dt [yr^{-1}]	–	–	–	0.069 ± 0.044	0.090 ± 0.044
dα/dt [yr^{-1}]	–	–	–	-0.218 ± 1.432	-1.543 ± 1.459
f_S	0.139 ± 0.002	0.167 ± 0.002	0.166 ± 0.002	0.162 ± 0.003	0.163 ± 0.003
f_B	0.193 ± 0.002	0.165 ± 0.002	0.166 ± 0.002	0.170 ± 0.003	0.169 ± 0.003

The fluxes f_S and f_B are normalized to $I = 18$ mag in OGLE-IV instrumental magnitude scale, or $I_{\rm std} = 18.085$ mag in calibrated I-band magnitudes.
In the "Parallax+Orbital" models, the parameter $\beta \equiv ({\rm KE/PE})_\perp$ is restricted to $\beta < 0.7$. See text.

4. Physical Parameters

4.1. Measurement of $\theta_{\rm E}$ *and* μ

We derive the source brightness from the model presented in Section 3 and derive the color from regression. We then find the offset from the clump on an instrumental color–magnitude diagram: $[(V-I),I]_s - [(V-I),I]_{\rm clump} = (-0.328, +3.990) \pm (0.023, 0.038)$. We adopt $[(V-I),I]_{\rm clump} = (1.06, 14.46)$ from Bensby *et al.* (2013) and Nataf *et al.* (2013), respectively, and so derive $[(V-I),I]_s = (0.732, 18.45) \pm (0.025, 0.063)$. We convert from V/I to V/K using the *VIK* color–color relations of Bessell and Brett (1988) and finally derive

$$\theta_* = 0.657 \pm 0.041 \ \mu{\rm as} \qquad (6)$$

using the color/surface-brightness relations of Kervella *et al.* (2004). Incorporating parameters from Table 1, we thereby derive.

$$\theta_{\rm E} = \frac{\theta_*}{\rho} = 1.40 \pm 0.09 \ {\rm mas}, \qquad \mu = \frac{\theta_*}{t_{\rm E}} = 8.1 \pm 0.5 \ {\rm mas/yr}. \qquad (7)$$

4.2. Masses, Distance, and Projected Separation

Combining the results of Section 4.1 and Table 1, we find

$$M = \frac{\theta_E}{\kappa \pi_E} = 0.234 \pm 0.026\ M_\odot \qquad m_p = \frac{q}{1+q} M = 4.4 \pm 0.5\ M_\oplus \qquad (8)$$

$$D_L = \frac{\text{a.u.}}{\theta_E \pi_E + \pi_s} = 0.86 \pm 0.09\ \text{kpc} \qquad a_\perp = s \theta_E D_L = 1.18 \pm 0.10\ \text{a.u.} \qquad (9)$$

where we have adopted a source parallax $\pi_s = 0.117 \pm 0.010$ mas and where $a_\perp$ is the projected separation. That is, the planet is a super-Earth orbiting a middle-late M dwarf. If we adopt a "snow line" scaled to host mass (*e.g.*, Kennedy and Kenyon 2008), and anchored in the observed Solar-system value, $a_{\rm snow} = 2.7$ a.u. $(M/M_\odot)$, then this planet lies projected at $a_\perp = 1.9\, a_{\rm snow}$.

5. Microlensing Earths and Super-Earths with Well-Measured Masses

OGLE-2017-BLG-1434Lb joins a small list of Earths and Super-Earths with well-measured masses discovered by microlensing. To be an "Earth or Super-Earth", we require a best-estimated planet mass $m_p < 7\ M_\oplus$. To be "well-measured" we set two requirements. First we require that the quoted 1σ error on the planet mass measurement span a factor < 2, *i.e.*, $\sigma(\log m_p) < 0.15$. Second, we require that the host mass was determined either by measuring both π_E and θ_E (as was done here) or by directly imaging the host.

We review the literature (effectively updating the summary by Mróz *et al.* 2017) and find only three such planets: OGLE-2016-BLG-1195Lb (Bond *et al.* 2017, Shvartzvald *et al.* 2017), OGLE-2013-BLG-0341LBb (Gould *et al.* 2014) and OGLE-2017-BLG-1434Lb (this work). In all cases, the mass determination is *via* measurements of θ_E and π_E. We note that there is another planet, MOA-2007-BLG-192Lb (Bennett *et al.* 2008, Kubas *et al.* 2012) whose host mass was quite well determined by direct imaging and whose best-estimated planet mass $m_p = 3.2^{+5.2}_{-1.8}$ falls in the defined range. However, the error bars on the planet mass are far too large to meet our criterion.

Table 2 gives the main characteristics of these systems.

T a b l e 2

Characteristics of Earth/Super-Earth Events

Event	$q(10^{-5})$	s	$M_{\rm p}/M_{\rm Earth}$	$M_{\rm h}/M_\odot$	$D_{\rm L}$ kpc	$a_\perp$/a.u.	$a_\perp/a_{\rm snow}$
OB161195	4.81	0.99	1.43	0.078	3.91	1.16	5.5
OB130341	4.60	1.00	2.00	0.145	1.16	0.88	2.2
OB171434	5.72	0.98	4.48	0.232	0.87	1.18	1.9

$a_{\rm snow} = 2.7$ a.u.$(M_{\rm h}/M_\odot)$

The first point to note about these three well-constrained low-mass planets is that they all have low-mass hosts, *i.e.*, from the hydrogen-burning limit to a middle-late M dwarf. The second point is that all are seen projected close to the Einstein ring, $s \approx 1$. And the third is that two of the three are extremely nearby, $D_L \lesssim 1$ kpc. All three of these characteristics are heavily influenced by selection, but none can be regarded purely as a selection effect.

As illustrated by Fig. 3, there are no microlensing planets with $q \lesssim 5 \times 10^{-5}$. This fact, combined with our sample requirement $m_p < 7\ \mathrm{M}_\oplus$, already implies that the hosts will be $M \lesssim 0.4\ \mathrm{M}_\odot$. However, as we will show in Section 6, the apparent "barrier" at $q \approx 5 \times 10^{-5}$ is not a selection effect: lower mass ratios could have been detected if such planets were common.

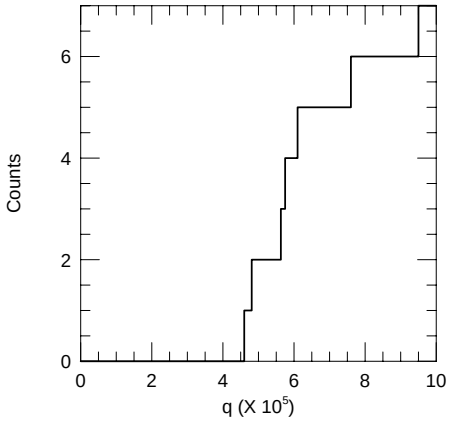

Fig. 3. Cumulative distribution of planet/host mass ratios q for the seven microlens planets with well-defined measurements $q < 10^{-4}$. Five of the seven have $4.6 \times 10^{-5} \leq q \leq 6.1 \times 10^{-5}$, suggesting either a rapid drop either in sensitivity of microlensing experiments to low mass-ratio planets or in the frequency of such planets.

Similarly, it is well-known that it is easier to detect planets when they lie projected close to the Einstein ring. In particular, for relatively high-magnification events, which applies to all three of these planets, planet-sensitivity diagrams have a triangular shape that is symmetric about $\log s = 0$ (Gould *et al.* 2010). However, since (as just mentioned) planets could have been detected at lower q, it follows immediately that they could also have been detected at higher $|\log s|$.

Finally, ground-based parallax measurements are heavily biased toward nearby lenses, simply because the microlens parallax is larger: $\pi_{\rm E} = (\pi_{\rm rel}/\kappa M)^{1/2}$. However, while this bias is quite strong for bulge lenses (to the point that there are no ground-based parallax measurements for events with unambiguous bulge lenses), it is only moderately strong for events of intermediate (few kpc) distance, and there are many ground-based parallax measurements for events at intermediate distances.

Thus, although this sample is heavily affected by selection, it does contain some information. Nevertheless, given that this sample is both small and biased by selection, we refrain from using it to draw any systematic conclusions.

6. Planet Mass-Ratio Function at the Low-Mass End

At $q = 5.8 \times 10^{-5}$, OGLE-2017-BLG-1434Lb is the eighth published microlensing planet with a planet/host mass-ratio measurement that places it securely in the range $q < 10^{-4}$. Strikingly, these are mostly clustered close to $q \approx 5 \times 10^{-5}$. See Fig. 3. This would seem to indicate a sharp cutoff either in sensitivity or in the existence of planetary companions at the separation ranges accessible to microlensing.

Because the discovery process of these planets is quite heterogeneous, it is not possible to reliably determine an absolute mass-ratio function from this sample. That is, there is no way to estimate the rate of non-detections from which this sample was drawn.

However, by applying the technique of "$V/V_{\rm max}$" (Schmidt 1968), we can use this sample to constrain the relative frequency by mass ratio. That is, we can consider various trial mass-ratio functions $F(q)$. For each detected planet i, we evaluate the "$V/V_{\rm max}$" ratio r_i defined by

$$r_i = \frac{\int_{q_i}^{q_{\rm max}} {\rm d}\ln q' F(q') P_i(q')}{\int_{0}^{q_{\rm max}} {\rm d}\ln q' F(q') P_i(q')} \tag{10}$$

where $q_{\rm max} = 10^{-4}$ (*i.e.*, the definition of the sample) and $P_i(q')$ is the probability that the planet would have been detected and published if the event had had exactly the same parameters as the actual one, but with a different $q' \neq q_i$.

If $F(q)$ has been chosen correctly, then the distribution of the r_i should be consistent with being drawn from a uniform distribution over the interval [0,1]. Hence, all trial mass-ratio functions $F(q)$ that yield a distribution of r_i that is inconsistent with uniform can be ruled out.

In principle, one might consider each P_i to be a continuous function varying between zero and one. For example, one might decide that $P_3(q' = 1.3 \times 10^{-5}) = 43\%$. That is, the light curve associated with the third event (and with the specified q') would have had a 43% chance of having been noticed as planetary in nature and then generating sufficient confidence in the evaluation to publish it. In fact, we will approximate the $P_i(q)$ as bi-modal, either 0 or 1. In most cases, this means that there is some continuous interval over which the planet is judged to be detectable, defined by $q_{{\rm min},i}$. Then Eq.(10) would become

$$r_i \rightarrow \frac{\int_{q_i}^{q_{\rm max}} {\rm d}\ln q' F(q')}{\int_{q_{\rm min},i}^{q_{\rm max}} {\rm d}\ln q' F(q')}. \tag{11}$$

However, as we will show, there is one event for which the range of discoverable planets could in principle have been discontinuous, so we retain the more general form of Eq.(10), at least at the outset.

6.1. Evaluation of $q_{\min,i}$ and $P_i(q')$

We define our sample by the following three criteria:

(1) Best-fit mass ratio $\log q < -4$,

(2) Formal error estimate $\sigma(\log q) < 0.15$,

(3) No alternate solutions with $\Delta\chi^2 < 10$ and $\Delta \log q > 0.3$.

Criterion (1) is the regime that we seek to probe. Planetary candidates that fail criterion (2) generally cannot be securely identified as being in the sample. Moreover, for planets with larger error bars, there is an increasing (and basically unknowable) probability that they would not be published. Candidates that fail criterion (3) are ambiguous in the sense that $q_{\min}$ can be substantially different for different solutions.

For consistency with these choices, we likewise set $P_i(q') = 0$ for any choice of q' that leads to failure of either criterion (2) or (3).

We find that one of the eight planets that satisfy criteria (1) and (2), fails criterion (3): OGLE-2017-BLG-0173 (Hwang *et al.* 2018). In fact, at the time that we devised these criteria, it was not yet known that OGLE-2017-BLG-0173 suffered from such a degeneracy. More generally, we did not alter our criteria as we studied the eight planets in detail. Even though one of these, OGLE-2017-BLG-0173, will be excluded from the sample, we include it in this part of the analysis for completeness and to explore the problems posed by this type of degeneracy.

Here we evaluate the range of q over which each of the eight planets that satisfy criteria (1) and (2) would have been detected. In each case we discuss the methods by which the planet was detected, or could have been detected using approaches that were applied to essentially all events in its class. "Detection" here requires that a simulated planet must meet two criteria: first, that it would have been noticed as a potential planet based on whatever data were routinely available, and second, that further analysis based on re-reduced data (plus whatever archival data would have been available) would have led to an unambiguous planet, worthy of publication. Because all the planets discussed here have low mass ratio q, we assume that if the planet was publishable, it would in fact have been published. (This is not actually true for some higher mass-ratio planets, which sometimes take many years to elicit enough enthusiasm to push through to publication.)

OGLE-2017-BLG-1434

OGLE-2017-BLG-1434 was first noticed as a potential planetary event by the MiNDSTEp collaboration based on its own data, as described in Section 2. If the mass ratio q had been somewhat lower, then MiNDSTEp data would have still shown a strong anomaly, and a similar alert would have almost certainly been issued. However, our concern here is to identify the lowest mass ratio q that would have yielded a noticeable signature, which would then trigger further investigation.

As we show below, at sufficiently low q, there would have been no noticeable deviations as seen from Chile, but there would still have remained significant deviations as seen from South Africa. In these limiting cases, there would have been no MiNDSTEp alert. The path to anomaly recognition would then have been the regular KMTNet review of ongoing events. This review would have combined OGLE online data with KMTNet "quick look" data. Hence, this is what we simulate below.

Fig. 4 shows the anomalous region of the light curve in on-line OGLE data and quick-look KMTNet data as it would have appeared with exactly the same parameters shown in Table 1, except with q taking on other values. To construct this figure, we measure the residuals from the best-fit model for each data point and renormalize the errors (with uniform error rescaling) so that $\chi^2/dof = 1$. Then for each observatory, we create a fake light curve whose value is the model light curve plus the residual in magnitudes, and whose error bar is the same as that of the original (renormalized) data point. In each case, we show both the original model and the model with different q that was used to construct the fake light curves. Note that the KMTNet "quick look" data consisted only of observations from field BLG41 (and not BLG01) and so are at half the cadence of the final KMTNet data that are shown in Fig. 1.

Fig. 4 has nine panels corresponding to $\log(q'/q) = -0.25, -0.5, \ldots -2.25$. Careful inspection of the $\log(q'/q) = -1.75$ panel shows clear systematic residuals, with two consecutive points below the point-lens curve, with the lower one being below by ≈ 0.3 mag. However, a cursory inspection would have shown only a single clearly outlying point. Based on the direct experience of the KMTNet team, we consider that it is possible that these would have triggered a further investigation, *i.e.*, first corroboration in the BLG01 data and, following this, re-reduction of all of the data. However, we judge that the probability for this is substantially below 50%, and hence within the framework we have adopted, we approximate this probability as $P = 0$. By contrast, the "quick look" data for $\log(q'/q) = -1.50$, with two points well below the single-lens curve, and one of them by ≈ 0.6 mag would certainly have triggered such an investigation. On the other hand, $\log(q'/q) = -2.0$ would certainly not have triggered such an investigation, but even it had, the re-reduced data would not have yielded a publishable detection because the signal is too weak.

To assess publishability, we first consider the marginally recognizable case, $\log(q'/q) = -1.75$. We model the fake re-reduced data in exactly the same way that we modeled the real data except that we exclude orbital motion (which would not be measurable for such a short and weak anomaly, and also would not be at all required for publication). We find that the planet's parameters in this case are well constrained, for example $\log q = -5.88 \pm 0.072$. This error bar is well within the limit set by criterion (2). We note that the best fit value (-5.88) differs by 1.4σ from the "input value" of the simulated data (-5.98). This difference re-

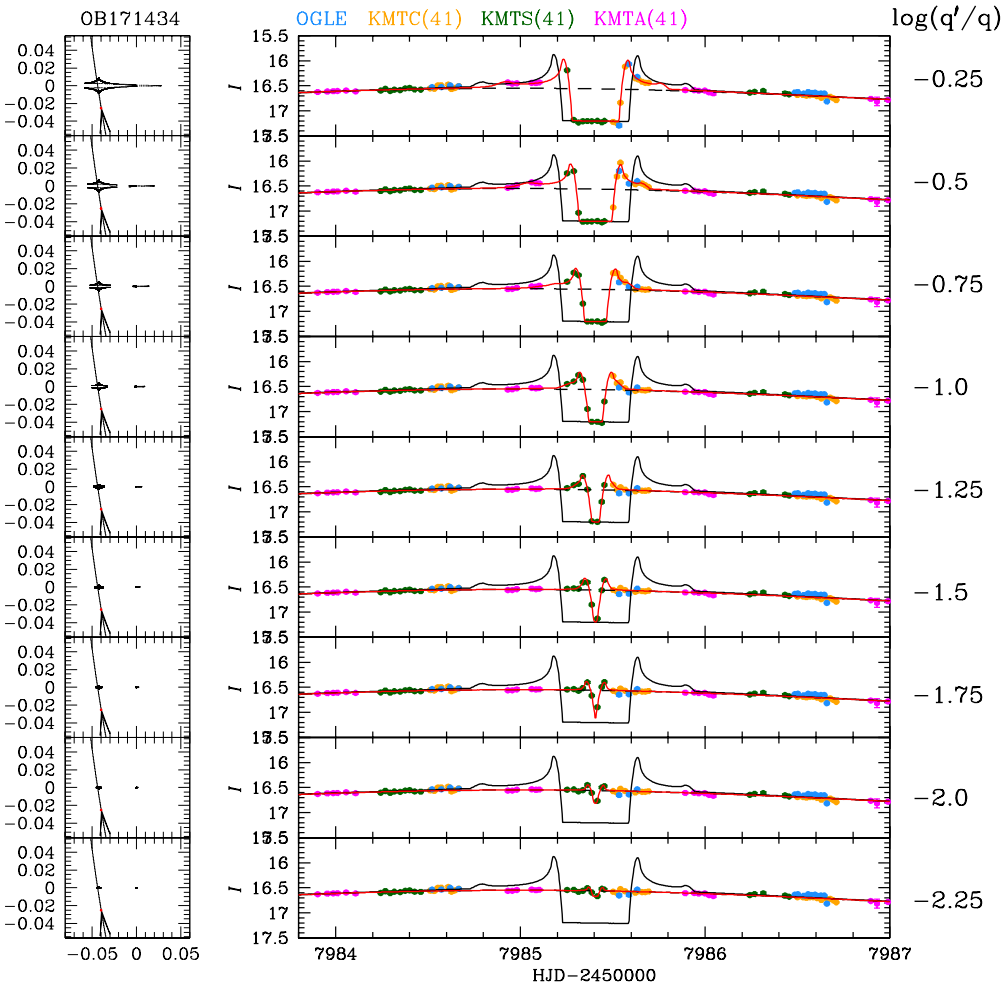

Fig. 4. Nine simulations of OGLE-2017-BLG-1434 with exactly the same parameters as the best-fit model (black curve) except that the mass ratio q is lower by $\Delta \log q$ as indicated in the right axis labels. In each case, the simulated data points (various colors) deviate from the model (orange curve) by exactly the same amount as the actual data points deviate from the best-fit model. The *left panels* show the corresponding caustic geometries. These characteristics will be same for all eight events in the figures that follow. The data points are based on the "online" OGLE data and "quick look" KMTNet data in order to focus on the problem of determining whether the event would be recognized as sufficiently interesting to trigger re-reductions.

flects the fact that the residuals, which concretely reflect the observational errors, are preserved in the simulated data. It follows that the much stronger signal at $\log(q'/q) = -1.50$ would also meet our criteria. We therefore adopt this threshold.

Before continuing, we note that more systematic procedures are currently being applied to 2017 KMTNet data, by means of which it is very likely that at $\log(q'/q) = -1.75$, this planet would ultimately have been discovered. That is, while the quick-look data were restricted to BLG41, all known microlensing events

(whether discovered by KMTNet or others) will by mid-2018 be reviewed using all available KMTNet data. However, such "ultimate discoveries" are irrelevant to the analysis being conducted here. All real planets that will "ultimately be discovered" are presently unknown, and thus are automatically excluded. Therefore, we must equally exclude simulated planetary events in this class.

OGLE-2017-BLG-0173

Hwang *et al.* (2018) analyzed OGLE and KMTNet data for OGLE-2017-BLG-0173 and found three solutions, including two "von Schlieffen" solutions (A,C) with $q \approx 6.5 \pm 0.9 \times 10^{-5}$, and one "Cannae" solution (B) with $q \approx 2.5 \pm 0.2 \times 10^{-5}$. All three solutions have $s \approx 1.5$. Two of these solutions (A,B) differ by only $\Delta\chi^2 = 3.5$, so this planet fails criterion (3), even though it satisfies criteria (1) and (2). Hence, this planet is excluded from our sample. Nevertheless, as mentioned above, we analyze it for completeness. Since solution (C) has $\Delta\chi^2 = 16$, we focus here on solutions (A,B).

As shown in their Fig. 1, the event betrays no hint of an anomaly in OGLE data, so the decision to examine quick-look KMTNet data was not influenced in any way by the presence of a planet. Thus, we must evaluate the minimum value of q that would have triggered a decision to re-reduce the data and then determine whether the resulting light curve would have been reliable enough to warrant publication of the (putative) planet. We note that, as shown in their Fig. 3, the "bump" in the KMTNet data was caused by the edge of a large source grazing the center of the caustic for solution (A) and by the center of a large source passing directly over the caustic for solution (B). Figs. 5 and 6 show sets of nine simulated light curves for $\log(q'/q) = -0.1, -0.2, \ldots -0.9$, for solutions A and B, respectively. The first point is that to the eye, the two figures look identical, except that the geometries at the left are quite distinct. Second, one sees that within each figure, the bump looks qualitatively similar in all cases, which is fundamentally due to the "Hollywood" (Gould 1997, Hwang *et al.* 2018) character of the event. The main difference is that the height of the bump scales $\propto q$ (as discussed by Hwang *et al.* 2018 see their Eqs.(9) and (10)). We estimate that at $\log(q'/q) = -0.7$ the "bump" (now 0.06 mag, compared to the actual one of 0.3 mag), would have still triggered a further investigation for either solution A or B. Further, the numbers at the right show $\Delta\chi^2 = \chi^2(\mathrm{1L2S}) - \chi^2(\mathrm{2L1S})$ between binary-source (1L2S) and binary-lens (2L1S) models. These values are certainly high enough to exclude the 1L2S interpretation.

However, we find that at $\log(q'/q) = -0.7$, and indeed at all q' shown in the figures, the analysis of either simulated data set (A or B) yields a discrete degeneracy between the two classes of models (von Schlieffen and Cannae), with $\Delta\chi^2 < 10$ and $\Delta \log q > 0.3$ between the two minima. That is, they all suffer from essentially the same degeneracy as the original event. Hence, although for $\log(q'/q) \geq -0.7$, we judge that they all would have been published (just as the original event was, Hwang *et al.* 2018), they all would have been excluded from the analysis.

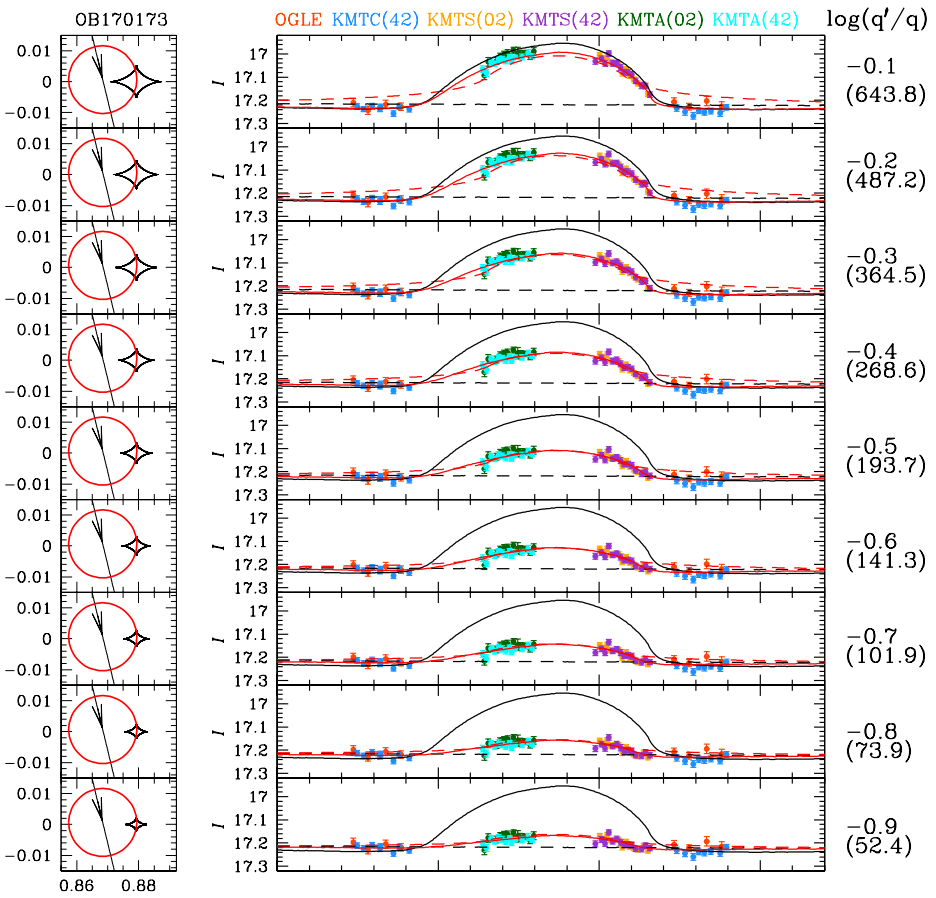

Fig. 5. Nine simulations of OGLE-2017-BLG-0173 (von Schlieffen solution A), similar to Fig. 4. The values in parentheses are $\Delta\chi^2 = \chi^2(1L2S) - \chi^2(2L1S)$, by which binary source models are excluded. To the eye, the degeneracy between these solutions and those in Fig. 6 (Cannae solution B) persists at all q.

This exclusion has no practical importance from the perspective of the present mass-ratio-function analysis, because the original event is itself excluded. However, the persistence of this degeneracy is of significant interest. Hwang *et al.* (2018) had noted that the other published Hollywood event, OGLE-2005-BLG-390 (Beaulieu *et al.* 2006), did not suffer from this von Schlieffen/Cannae degeneracy. And they further noted that the caustic was much smaller than the source in that case, whereas the caustic was of comparable size to the source for OGLE-2017-BLG-0173. They therefore conjectured that the degeneracy was a consequence of the caustic size relative to the source size. However, the present analysis shows that this is clearly not the case. Hence, there must be some other governing factor. This may be the angle of the source trajectory, α, but investigation of this question is well outside the scope of the present work.

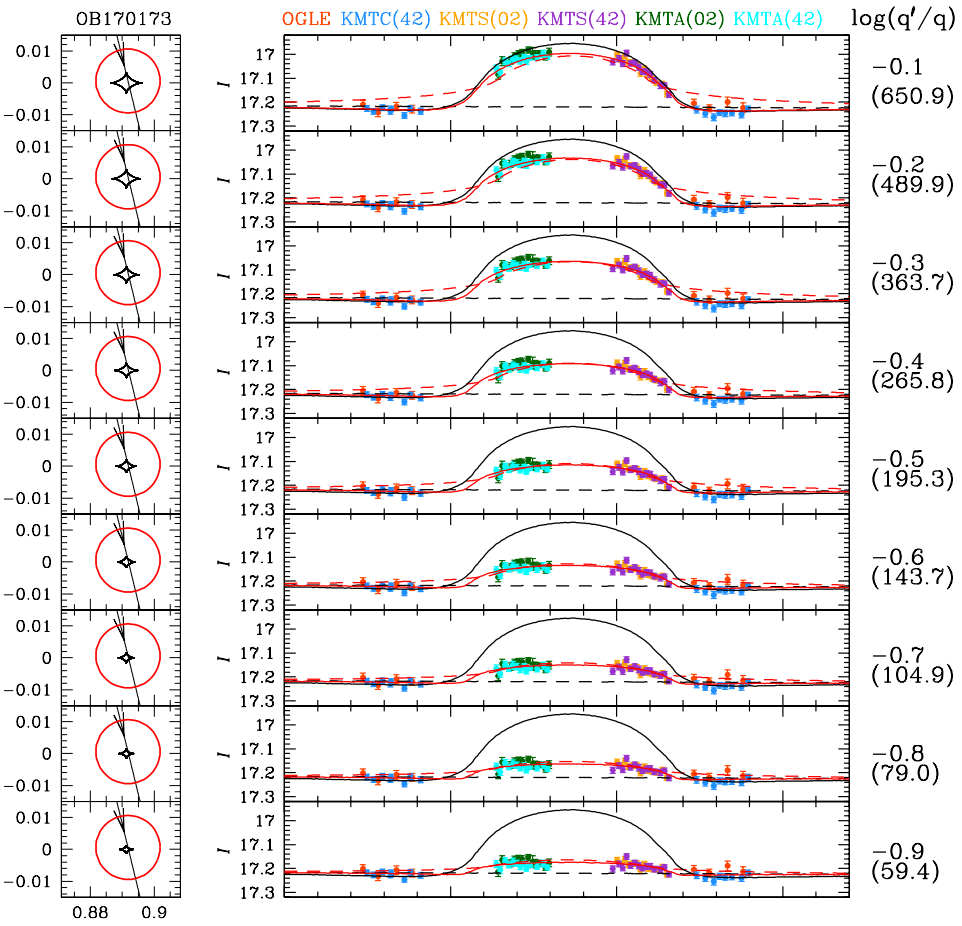

Fig. 6. Nine simulations of OGLE-2017-BLG-0173 (Cannae solution B), similar to Fig. 4. The values in parentheses are $\Delta\chi^2 = \chi^2(1L2S) - \chi^2(2L1S)$, by which binary source models are excluded. To the eye, the degeneracy between these solutions and those in Fig. 6 (von Schlieffen solution A) persists at all q.

OGLE-2016-BLG-1195

OGLE-2016-BLG-1195 was analyzed by two groups (Bond *et al.* 2017, Shvartzvald *et al.* 2017) based on completely different data sets. The two groups obtained slightly different mass-ratio estimates $q = 4.22 \pm 0.65 \times 10^{-5}$ (Bond *et al.* 2017) and $q = 5.60 \pm 0.75 \times 10^{-5}$ (Shvartzvald *et al.* 2017). Here we adopt a weighted average $q = 4.81 \pm 0.49 \times 10^{-5}$.

The anomaly in this event was discovered and publicly announced by the MOA collaboration in real time, *i.e.*, at UT 15:45 June 29, 2016. In fact, while the internal discussions that led to this alert were still ongoing, the MOA observers increased the cadence of observations, beginning at UT 15:15. That is, prior to this change, MOA observed the field steadily at a cadence of $\Gamma = 4.0\ \mathrm{hr}^{-1}$, which is their normal

cadence for this field, whereas between UT 15:15 and UT 16:48 (roughly the "end" of the anomaly), the field was observed 16 times, for a mean cadence of $\langle\Gamma\rangle = 10.3\ \mathrm{hr}^{-1}$. A slightly lower cadence continued for the rest of the night. See Bond *et al.* (2017).

Hence, in contrast to the previous two cases, one must consider two possible data streams for any mass ratio q': the actual one (in the case that the observers would have recognized the anomaly and so taken the initiative to increase the cadence) and one in which the anomaly was not recognized, so the cadence remained at the standard $\Gamma = 4.0\ \mathrm{hr}^{-1}$. Fortunately, as we show below, the two cases lead to very similar conclusions. This is partly because the anomaly had already peaked when the cadence was changed and partly that there existed an independent data set from KMTA.

We first focus on the more conservative case, *i.e.*, that at sufficiently low q', the observers would not have recognized the anomaly. This leads us to construct a "thinned" version of the MOA online data set that is consistent with the normal MOA cadence. For the times that MOA observed the field two, three or four times consecutively (in 1.5 min intervals), we always choose the second of these observations. For the remaining observations, we thin them so that the surviving observations are as closely spaced to 15 min as possible. In particular, we keep six observations from the 16 observations during the final 93 min of the anomaly.

Then, under either assumption (real-time anomaly recognition or not), and as for the two other events previously examined, we address two questions, whether the anomaly would ultimately have been recognized and, if so, whether the re-reduced data would have yielded a reliable planet detection. A very important difference from the previous two cases, however, is that the full extent of the anomaly was continuously observed by two different surveys, MOA (Bond *et al.* 2017) and KMTA (Shvartzvald *et al.* 2017), from sites separated by several thousand km. The data quality was overall roughly comparable (judged by the quoted errors of parameters). Hence, the normal caution that a low-amplitude signal might be due to unknown systematics would not apply to this case, since the same signal would be present in both data sets. Moreover, even though the actual analyses were done in two separate papers, a joint paper combining both data sets would have been written if neither data set was by itself adequate for publication.

As noted above, the first threshold is simply recognizing the anomaly. This need not have been in real time. In principle, it could have been recognized later in either the MOA or KMTNet data. However, in contrast to the two cases discussed above, the 2016 quick-look KMTNet data were of substantially lower quality, and tests show that the anomaly would not have been recognized according to the procedures followed in that year. Hence we should examine only the on-line MOA data. We note that the event was a Spitzer microlensing target (Shvartzvald *et al.* 2017), part of a broader program to measure the Galactic distribution of planets (Gould *et al.* 2015a,b, Yee *et al.* 2015, Calchi Novati *et al.* 2015, Zhu *et al.* 2017),

and therefore the MOA data would have been examined quite closely even if the anomaly had not been detected in real time.

Following the above considerations, we examined fake light curves constructed on the basis of MOA online data, both with and without the additional MOA points triggered by the alert. We are confident that the anomaly would have triggered re-reductions of MOA and KMTNet data for $\log(q'/q) = -0.3$ and perhaps even lower. However, we do not investigate the exact threshold, nor do we show the plots that we reviewed because, as we now describe, the fundamental issue is not simply recognizing that there was an anomaly.

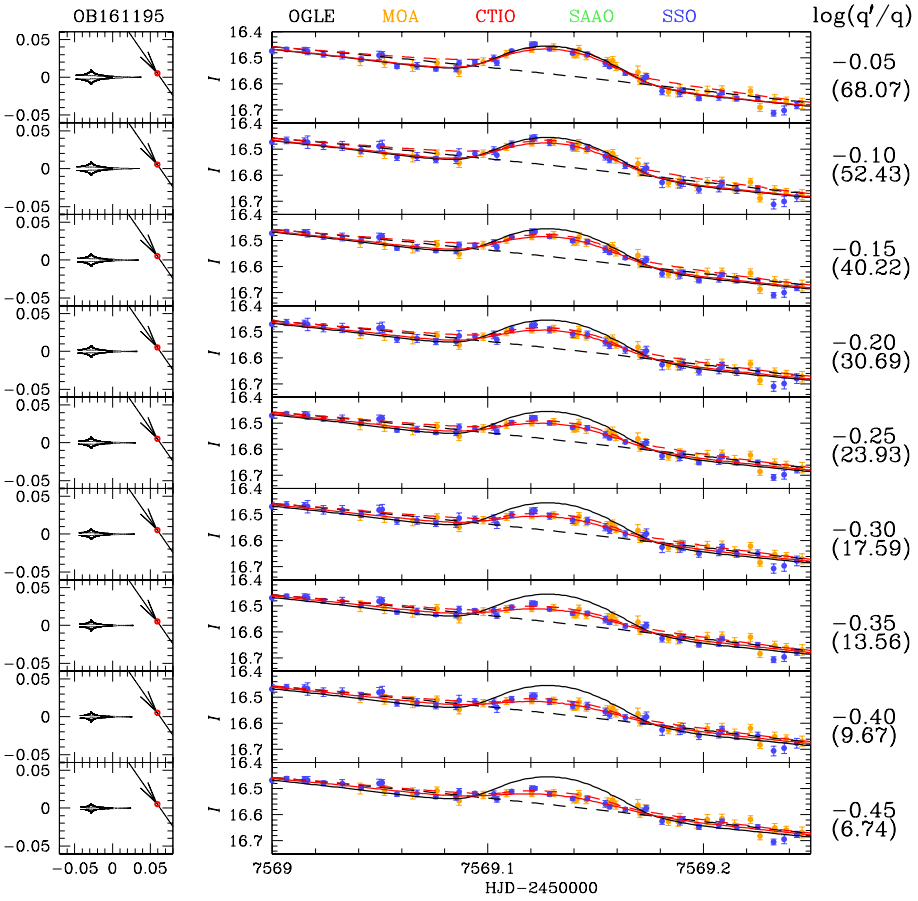

Fig. 7. Nine simulations of OGLE-2016-BLG-1195, similar to Fig. 4, except that in this case the data points are based on the re-reduced data in order to focus on whether the event (once recognized as interesting) would be publishable.

Fig. 7 shows 9 panels with $\log(q'/q) = -0.05, -0.10, \ldots -0.45$, with re-reduced data from both MOA and KMTA. In each panel, we show both the planetary (2L1S) and binary source (1L2S) models. The number in parentheses to the right of each panel gives the $\Delta\chi^2 \equiv \chi^2(1L2S) - \chi^2(2L1S)$ difference between these models. For

$\log(q'/q) = -0.30$, -0.35, and -0.40, these are 17.6, 13.6, and 9.7 respectively. Given that two independent data sets are contributing to these values and that neither shows any sign of systematics, we conclude that the first two would be considered adequate for a reliable detection of a planet, while the third would not.

Next, we address the role of the real time alert. If the event were not recognized in real time at lower mass ratio (as it was in the actual case) then the only difference in the evaluation of publishability would be the "exclusion" of ≈ 10 MOA points during the second half of the anomaly (plus some post-anomaly points), which would imply slightly lower $\Delta\chi^2$. In particular, for $\log(q'/q) = -0.30$ and -0.35, $\Delta\chi^2 = 13.1$ and 10.2, respectively. By the argument just given, these would render the first as a publishable planet and the second not. Hence, the only relevant question about real-time alerts is whether, at $\log(q'/q) = -0.35$, the event would have been alerted based on the online MOA data. Given that the actual event was not recognized by the observers until the deviation was nearly at peak, and so with roughly twice the deviation as the $\log(q'/q) = -0.35$ case, we regard this as highly unlikely. Thus, we conclude that the threshold for detection/publication is $\log(q'/q) = -0.30$.

Finally, we analyze the simulated $\log(q'/q) = -0.30$ as though it were a real event. We find that there is a unique minimum and that $\sigma(\log q) = 0.10$. Hence, it clearly meets our criterion (2).

OGLE-2013-BLG-0341

OGLE-2013-BLG-0341 was originally recognized as having a minor-image planetary anomaly at $\mathrm{HJD}' = 6393.7$ based on real-time OGLE data, four days after the anomaly, when A.G. cataloged it as a possible high magnification event and therefore carefully examined the light curve as part of his assessment. He publicly announced this but also noted that since the lower limit on the magnification, $A_{\rm max} > 10$, was not particularly high, no immediate action was warranted. However, from this point on, the event was closely monitored with the aim of organizing intensive follow-up observations near peak, if indeed its prospective high-mag character was confirmed. Such intensive observations were in fact initiated ten days after the anomaly and about two days before peak. The peak was characterized primarily by a binary (not planetary) caustic. However, Gould *et al.* (2014) later showed that the planet's parameters could be recovered even when the data points in the vicinity of the planetary anomaly (144 points to be precise) were removed from the data.

The initial recognition of the planetary dip can be partially attributed to chance. The purpose of A.G.'s review of the online OGLE light curves was not to find planetary anomalies, but rather high-magnification events that could be intensively monitored to find planets near peak (Gould *et al.* 2010). Thus, it was hardly guaranteed that the actual signal would have been noticed when it was, and it is fairly unlikely that it would have been noticed at this point if the dip had been only half as deep.

Nevertheless, because the event eventually did become high-magnification, the light curve would have been singled out for extremely close inspection, regardless of whether a planetary anomaly had previously been noticed or not. If the planet had been noticed at this point, then of course exactly the same follow-up observations would have been initiated. If not, then when the event showed very obvious binary-like behavior (see Fig. 1 of Gould *et al.* 2014), the event would have been abandoned as "not interesting". Hence, the signature from the planet in the caustic exit would have been drastically reduced due to lack of follow-up data[4].

In brief, an important (though as we shall see, not only) question of whether the planet would have been recognized comes down to: would Gould *et al.* (2014) have recognized the planetary signature once they began closely examining this high-mag event, as it approached peak?

Fig. 8 shows nine panels with $\log(q'/q) = -0.05, -0.10, -0.15, -0.2, -0.3, -0.4, -0.5, -0.75, -1$. This event is unique in our sample in that as q declines, the anomaly becomes less visible and then invisible, but then begins to become more visible again at $\log(q'/q) = -0.3$. Then, at $\log(q'/q) = -0.5$, its visibility peaks, whereupon it gradually declines. The reason for this behavior is that in the actual event, the source passed along the trough between the two triangular, minor-image caustics, but very close to one of the caustic walls. The source trajectory relative to the mid-line of the trough remains basically the same as q declines, but because the triangular caustics move closer together, the edge of the source moves increasingly over the caustic wall. At first, the excess magnification of the limb increasingly cancels the dip due to the main part of the source passing through the trough. However, when q falls sufficiently, the excess magnification starts to dominate, and there is a bump in place of the trough.

The scatter in the OGLE online data for the six points on the night of the anomaly is small, $\sigma = 0.03$ mag. Hence, a mean deviation of just 0.06 mag would be a five-sigma detection, which we regard as the minimum needed to be both recognizable by eye and to engender sufficient confidence to trigger a massive follow-up campaign, as discussed above. This threshold has already been crossed at $\log(q'/q) = -0.15$ for the "fading" dip. It is crossed again for the "rising" bump at $\log(q'/q) = -0.3$ and then is crossed again for the "fading" bump slightly be-

[4]With respect to the coverage of the caustic, both the OGLE and MOA "survey" data must be treated substantially as "follow-up". For the night of the caustic, MOA increased its cadence from its normal level of $\Gamma = 3.5$ hr^{-1} to $\Gamma = 20$ hr^{-1}. For OGLE, the role of the alert was somewhat more involved. OGLE-2013-BLG-0341 lies close to the edge of the OGLE chip BLG501.12. Hence, it tended to drift off toward – and then over – the edge of the chip over the course of a given night, until the telescope pointing was reset. Thus, for example, the sixth and final point on the night of the "dip" was at HJD$' = 6393.717$, whereas other events in this field had nine additional points on this night ending at HJD$' = 6393.909$. The pointing for this field was specially adjusted on the night of the caustic exit, which probably roughly doubled the number of OGLE points that night relative to what would have occurred in the absence of an alert. Hence, the alert accounted for not only 100% of the data from non-survey telescopes, but also 82% of the MOA data and 50% of the OGLE data. Only the Wise survey was unaffected by the alert.

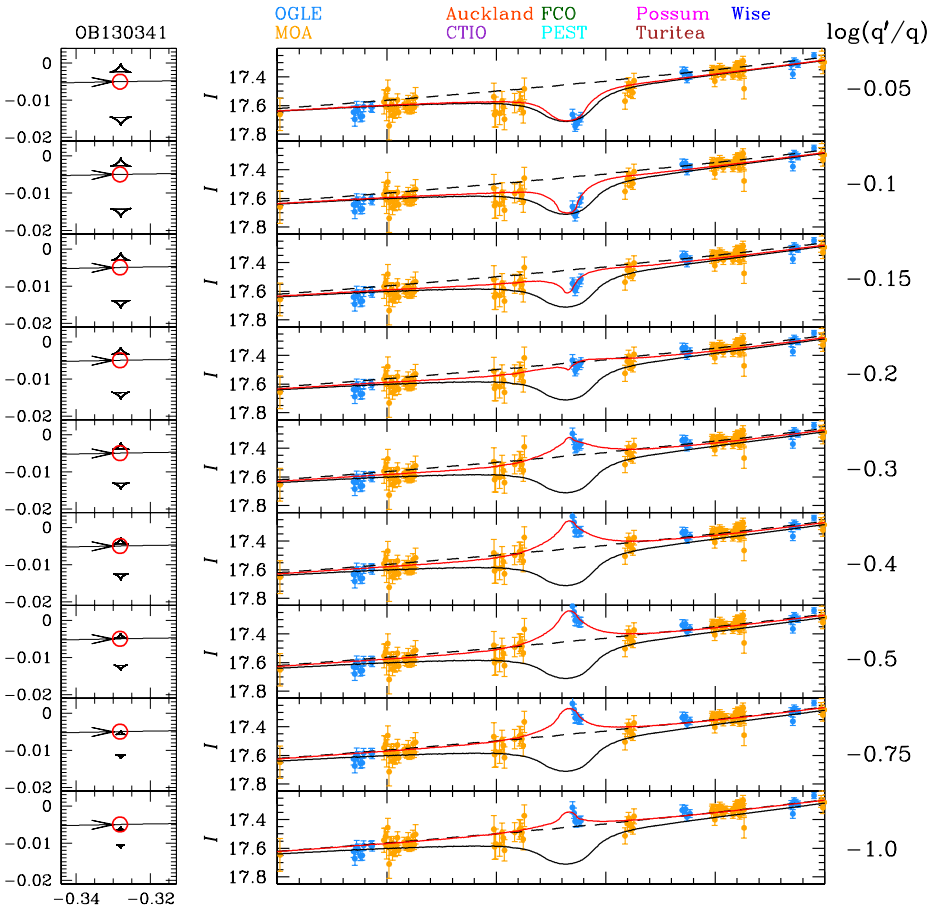

Fig. 8. Nine simulations of OGLE-2013-BLG-0341, similar to Fig. 4. Similar to those simulations, it is based on "online" OGLE and MOA data in order to focus on the problem of real-time recognition of the planetary anomaly.

low $\log(q'/q) = -0.75$. We conclude that follow-up observations would have been triggered in the two ranges $(\log(q'/q) > -0.1)$ and $(-0.3 > \log(q'/q) > -0.75)$.

Nevertheless, we now argue that only in the former range would a paper claiming secure detection of a planet have been written. First, in contrast to a dip in the light curve (which can only be explained by a minor-image anomaly), an isolated bump in the light curve can also be explained by a 1L2S solution. The OGLE anomaly data are confined to a narrow range in time, and so have no leverage on the shape of the bump to distinguish between 2L1S and 1L2S.

In principle, the follow-up data (which we argued above would have been triggered for the second – "bump" – range of q) could have confirmed the planetary nature of the anomaly. However, there are two practical issues that severely undermine this possibility. First, at our finally adopted value of $\log(q'/q) \leq -0.1$, we find that this confirmation is already relatively weak, $\Delta\chi^2 = 66$, a point to which

we return below. More fundamentally, it is very unlikely that the analysis would have been pushed to the point that the test would have been devised of deleting the planetary-anomaly data. The analysis of the event was quite complex and required enormous human and computer resources. It was only in the process of carrying out this analysis that it was discovered that such confirmation was possible. Hence, the motivation to analyze an event to this level in the case that there was a (seemingly) unassailable non-planetary interpretation would almost certainly have been lacking. Finally, even supposing that such an analysis were done, the "confirmation" of $\Delta\chi^2 < 50$ would almost certainly not have been regarded as sufficient to claim a secure detection. This is reflected in the fact that Gould *et al.* (2014) specifically argued that the unambiguous planetary anomaly (due to the fact that it was a minor-image dip) served as "confirmation" that the subtle – and by eye, invisible – deviations in the binary caustic could be regarded as a reliable indicator of a planet. Without such independent knowledge, and at relatively low $\Delta\chi^2$, this would have at best led to the reporting of an interesting planetary candidate.

We conclude that the threshold for planet detection is $\log(q'/q) = -0.10$. We confirm that this solution is unique and find $\sigma(\log q) = 0.04$, implying that our sample criteria are satisfied at this threshold[5].

MOA-2009-BLG-266

MOA-2009-BLG-266 (Muraki *et al.* 2011) was recognized as having a potentially planetary anomaly in real time by the MOA collaboration at the end of the New Zealand night from the sharp decline in the previously smoothly rising light curve. This triggered follow up observations at many sites, which further articulated the decline, mapped the trough and then the rise. The basic model of the event was already derived before any of these follow-up data were taken, let alone reduced, so that in the actual case, the alert-generated data were needed for full characterization of the planet, but not for its discovery. However, if the mass-ratio had been lower, it is possible that the planet could not have been characterized well enough to warrant publication in the absence of the follow-up data. Thus, for this event, it is especially important to evaluate both how well the planetary perturbation could have been recognized in real time, and how well the planet could have been characterized with, and without, follow-up observations.

We note that five different observatories took data on MOA-2009-BLG-266 prior to the alert, of which four also took data after the alert. Hence, one must assess whether these four would have taken data in the absence of the alert. We find that only one of these (Canopus) took data in a way that indicated sustained

[5]We note that OGLE-2013-BLG-0341 was part of the Shvartzvald *et al.* (2016) sample of events that were jointly monitored by the OGLE, MOA, and Wise surveys. All such events were examined extremely closely by Y.S., so that it is possible that the planetary anomaly would have been noticed after the event was over, even if it were missed prior to the peak. In this case, however, there would have been no follow-up data and therefore only extremely weak confirmation of the planet from the binary caustic.

focus on the event as it approached peak: they took four points spread over 1.4 hr on the night before the alert. The others either took one point on occasional nights or had stopped taking data altogether. Thus, it is reasonable to suppose that Canopus would have also taken four points on the next night, even if there had been no alert. However, these data would have overlapped MOA data and so would not have qualitatively altered how well the event could have been characterized in the absence of an alert (and so absence of data in the trough).

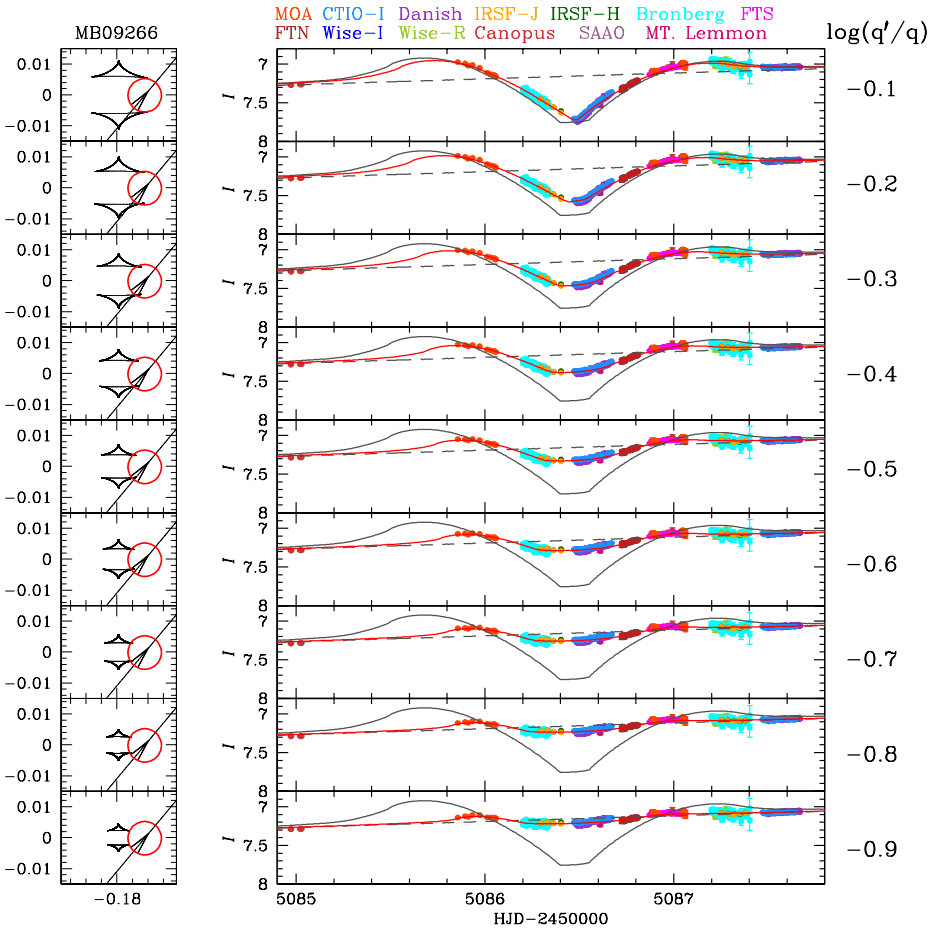

Fig. 9. Nine simulations of MOA-2009-BLG-266, similar to Fig. 4. The simulations are based on re-reduced data from all observatories.

Fig. 9 shows nine panels with $\log(q'/q) = -0.1, -0.2, \ldots -0.9$ and all data re-reduced. The first question is whether, with a smaller mass ratio, MOA would have issued an alert (based, of course, on online data). While Fig. 9 shows re-reduced data, it still enables us to understand how the basic form of the MOA light curve evolves as q declines: over the range $\log(q'/q) \leq -0.6$, it basically takes the form of a mean excess over the point-lens model (dashed line). We now argue that an

anomaly of this form would give rise to an alert provided that the mean excess over the predicted point-lens light curve was 0.1 mag.

Based on the MOA online data from before the night of the anomaly, we find that one can predict the flux (based on a point-lens model) on the night of the anomaly to 0.085 mag at 3σ confidence. There are ten MOA points on that night, with scatter 0.024 mag. Hence a standard error of the mean of 0.008 mag. Thus, a mean offset of 0.1 mag would yield a $\Delta\chi^2 \approx 12$ discrepancy, which would be sufficient indication to issue an alert. This condition is satisfied for $\log(q'/q) = -0.6$, but not lower mass ratios. At higher mass ratios, the mean offset itself satisfies this condition, and in addition there is increasing evidence of a decline (which is what triggered the actual alert).

We fit simulated data for the case $\log(q'/q) = -0.6$, and find that the solution is both unique and well localized ($\sigma(\log q) = 0.02$). We then repeat this exercise for $\log(q'/q) = -0.7$ but with only MOA and Canopus data (since, as we argued above, there would be no alert and hence no follow-up data apart from Canopus). We find that there are several local minima from the broad search of parameter space, and that none of the models derived at these minima appear compelling enough to warrant publication.

We conclude that the threshold for this event is $\log(q'/q) = -0.6$.

OGLE-2007-BLG-368

The details of the anomaly alert of OGLE-2007-BLG-368 are recounted by Sumi *et al.* (2010). The first alert was given by the robotic SIGNALMEN anomaly detector (Dominik *et al.* 2007) $\mathrm{HJD}' = 4302.314$, being triggered by the nine MOA points that lie ≈ 0.2 mag below the point-lens model. This alert prompted follow-up observations beginning five hours later in Chile by the μFUN SMARTS 1.3-m telescope and the PLANET Danish 1.5-m, and then from additional telescopes continuing toward the west. From the present perspective, it is important to note that this alert did not reach the MOA observer and so did not influence the cadence of MOA observations on the night $\mathrm{HJD}' \approx 4303$. These were the next observations after those in Chile. Hence, the next observations that were influenced by the alert (after Chile) were from the PLANET Canopus observations from Tasmania, whose three closely spaced points basically overlap the last MOA point. There were additional follow-up observations, which played an important role in characterizing the actual event, but as we will show, these play very little role in the current $V/V_{\max}$ analysis.

Fig. 10 shows nine panels with $\log(q'/q) = -0.1, -0.2, \ldots -0.9$ and all data re-reduced. Note that for $\log(q'/q) \leq -0.4$, the point-lens model and the planetary model are nearly identical for the follow-up data taken $\mathrm{HJD}' > 4303.3$. That is, only the μFUN Chile, Danish Chile, and Canopus data would have played a significant role for $\log(q'/q) \leq -0.4$.

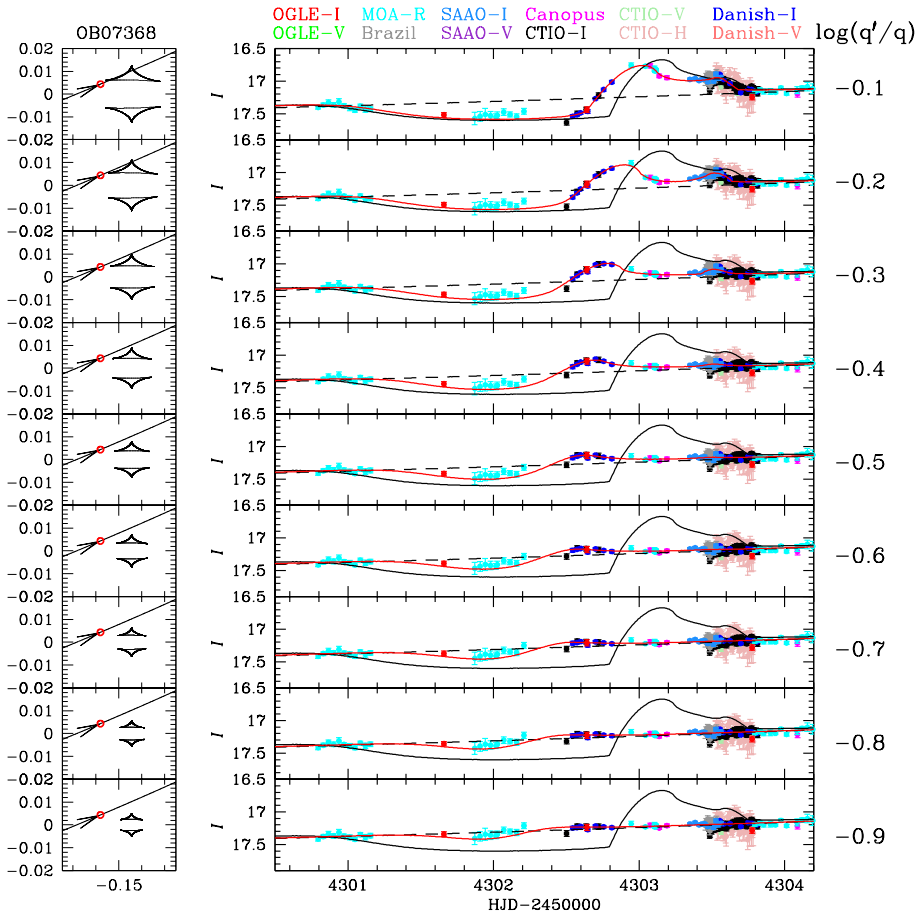

Fig. 10. Nine simulations of OGLE-2007-BLG-368, similar to Fig. 4. This figure is based on re-reduced data from all observatories. It should be compared to the next one (Fig. 11), which is based on "online" OGLE and MOA data.

Fig. 11 shows the same nine panels as Fig. 10 but with only online survey data. Based on this figure, we consider it to be unlikely that there would have been an alert on this event in time to trigger CTIO observations for $\log(q'/q) \leq -0.4$. Moreover, we can say with near certainty (since A.G. made this decision) that CTIO would not have responded to such an alert if it had been given. However, the CTIO response is of secondary importance because the Danish data, which cover the same time interval, would certainly have been taken.

As usual, we first ask at what threshold would the online survey data have led to re-reductions, and then ask whether these reductions would have led to a publishable result given the data that would have been acquired.

The online OGLE data would, by themselves, certainly have triggered re-reductions at $\log(q'/q) \geq -0.4$. At $\log(q'/q) = -0.5$ this is less probable, but in this case the partial corroboration from online MOA data would have almost certainly led to re-reductions. Re-reduction at $\log(q'/q) = -0.6$ is also a possibility.

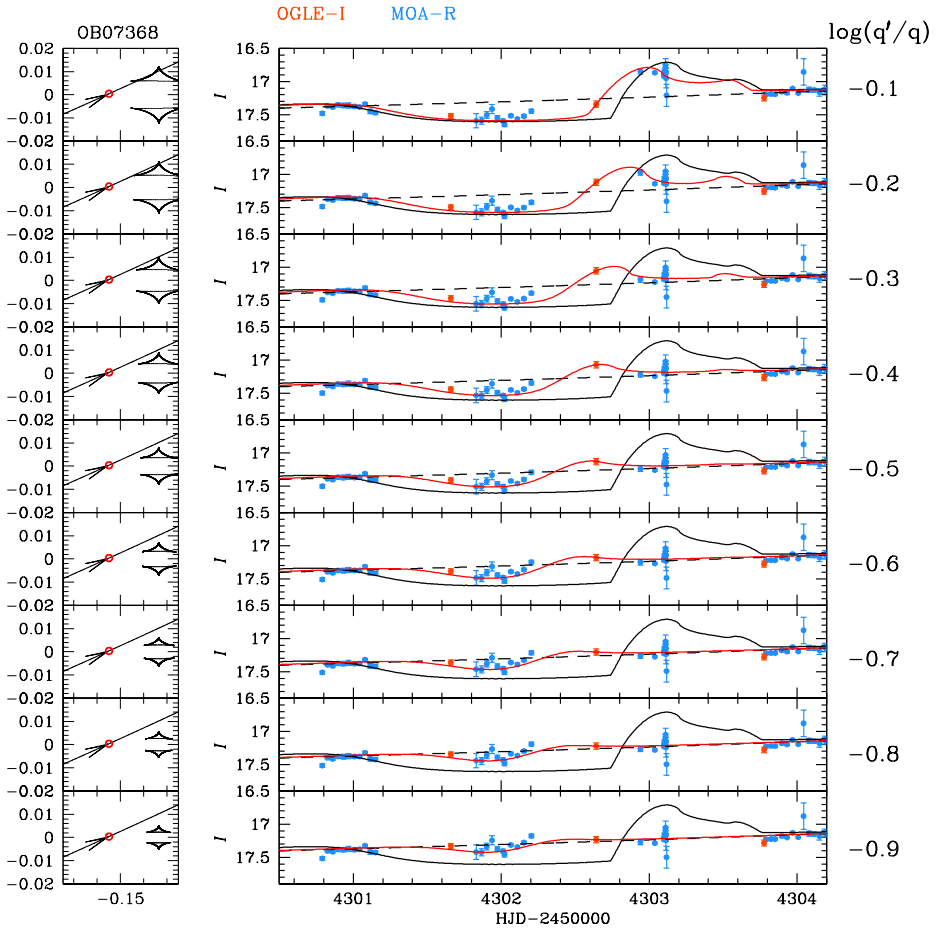

Fig. 11. Nine simulations of OGLE-2007-BLG-368, similar to Fig. 4. This figure is based on "online" OGLE and MOA data. It should be compared to the previous one (Fig. 10), which is based on re-reduced data from all observatories.

Recall that at $\log(q'/q) = -0.3$, we concluded that there would have been an anomaly alert. We analyze all data and find that the solution is well-localized with $\sigma(\log q) = 0.025$. At $\log(q'/q) = -0.4$, we must consider two cases, *i.e.*, with and without the alert (and so follow-up data). We find that with the follow-up data, the minimum is well localized with $\sigma(\log q) = 0.08$, so satisfying all our criteria. However, with survey-only (re-reduced) data, we find that there are two minima separated by $\Delta\chi^2 < 10$ and $\Delta \log q > 0.3$, which would fail our third criterion. Since we assessed that there would probably not be an alert at $\log(q'/q) = -0.4$, we conclude that the threshold for detection is $\log(q'/q) = -0.3$. We recognize that there is some probability of an alert at $\log(q'/q) = -0.4$, and therefore (according to the analysis just given) of a publishable detection. However, since we are approximating probabilities P as either zero or one, we simply adopt the threshold $\log(q'/q) = -0.3$.

OGLE-2005-BLG-390

OGLE-2005-BLG-390 was detected primarily in follow-up data organized by the PLANET collaboration, but in contrast to all previous cases, all of these data were taken in response to an alert of the microlensing event itself, not an anomaly (Beaulieu *et al.* 2006). The anomalous behavior was noted by the observer at the Danish telescope in Chile, and in principle this could have influenced other observatories farther to the west. PLANET conducted (but did not formally report) an investigation of this question at the time and found that their internal alert did not induce changes in the observing cadence at Canopus (in Tasmania), but did lead to an increased cadence at Perth. However, from the actual record of observations, the observational cadence at Perth did not in fact change from what it had been on previous nights. While in principle it is possible that the internal alert caused a previous decision to reduce the cadence to be exactly revsersed, there is no specific report of such a coincidence. Hence, we believe a more likely explanation is that

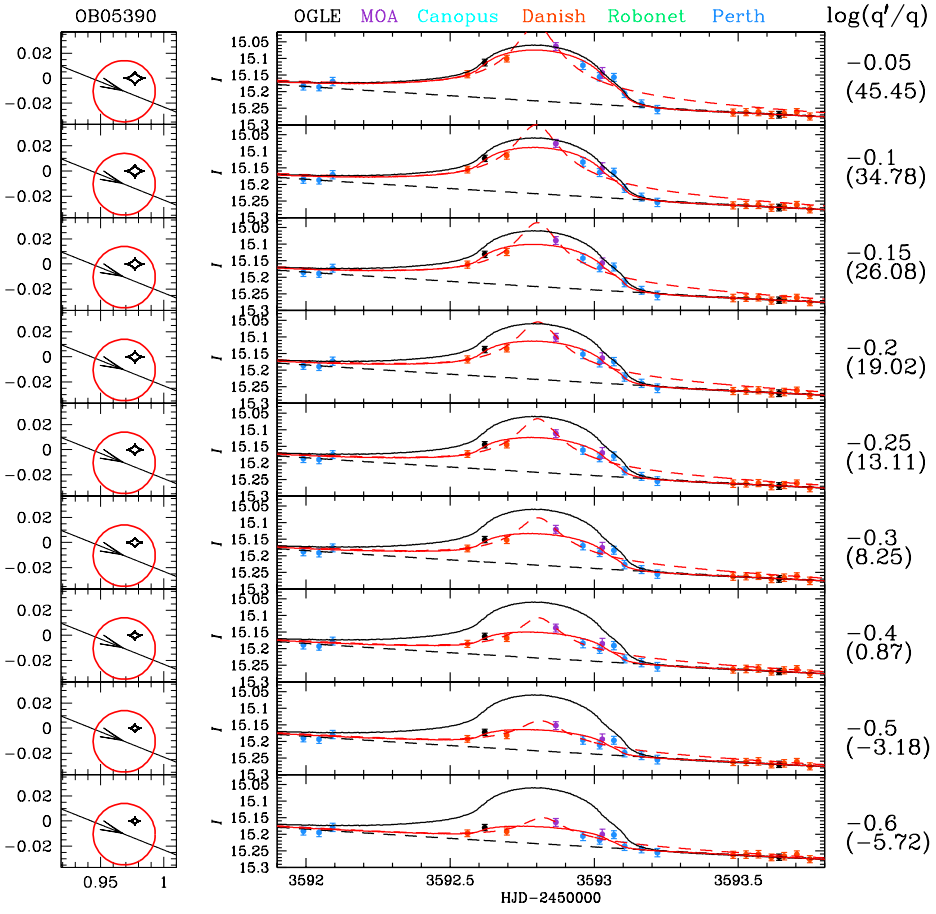

Fig. 12. Nine simulations of OGLE-2005-BLG-390, similar to Fig. 4. It is based on re-reduced data from all observatories.

the cadence was actually unaffected by the alert. In any case, as we will show below, the threshold value of q' for detection (even assuming no impact of the internal alert) is only slightly below the mass ratio q of the actual event, so that it is very likely that an internal alert would have been issued at this threshold. That is, taking both factors together, the probability that the observations would have been the same for an event at threshold is much greater than 50%. Therefore, following our general procedure of treating $P(q)$ as bi-modal (see Eq. 11), we proceed under the approximation that the same observations would have been taken over the anomaly whether a planetary signal was suspected to be present or not.

Fig. 12 shows nine panels with $\log(q'/q) = -0.05, -0.10 \ldots, -0.30, -0.40, -0.50, -0.60$ and all data re-reduced. This event was one of relatively few monitored by the PLANET collaboration, and hence the data would have been very closely inspected even if the anomaly had not been noticed in real time. Thus, the anomaly would have been easily noticed at $\log(q'/q) = -0.5$ and probably somewhat below. However, as we now show, it is not important to evaluate the exact boundary of this recognition.

Because the anomaly is a smooth bump, it can potentially be fit as a binary source event, 1L2S. In the actual event, this degeneracy was investigated and ruled out both by $\Delta\chi^2 = 46$ and also by obvious deviations in the light curve from the 1L2S model. However, for $\log(q'/q) = -0.25$, we see that 2L1S is favored over 1L2S by only $\Delta\chi^2 = 13$. For the case of OGLE-2016-BLG-1195, we regarded this value as marginally acceptable because there were two independent data sets that spanned the entire anomaly. However, in the present case, which lacks such confirmation, we regard it to be marginally unacceptable and therefore adopt a threshold of $\log(q'/q) = -0.2$. We find that at this threshold, $\sigma(\log q) = 0.11$, which satisfies our sample criterion $\sigma(\log q) < 0.15$.

OGLE-2005-BLG-169

The overwhelming majority of evidence for a planet in the OGLE-2005-BLG-169 data lies in the extremely intensive follow-up data taken from the MDM observatory in Arizona, beginning very close to the peak of the event (Gould *et al.* 2006). As with all data in and near the anomaly of this event, these were obtained without reference to the possible existence of a planet. Because the dense data began near peak, there was a modest ambiguity in the solutions presented by Gould *et al.* (2006). This was resolved by the analyses of Bennett *et al.* (2015) and Batista *et al.* (2015) when they, respectively, partially and fully resolved the lens 6.5 yr and 8.2 yr after the event. Here we use their parameters for the event, in particular $q = 6.1 \times 10^{-5}$. Fig. 13 shows nine panels with $\log(q'/q) = -0.2, -0.4, \ldots -1.8$, with all data re-reduced.

Because of the unprecedented character of the data set, roughly 1000 high-precision data points (later binned to 137) taken over three hours, the data were examined extremely closely. Although the deviation from a point lens was noticed very quickly, submission of the manuscript was delayed for 10 months, primar-

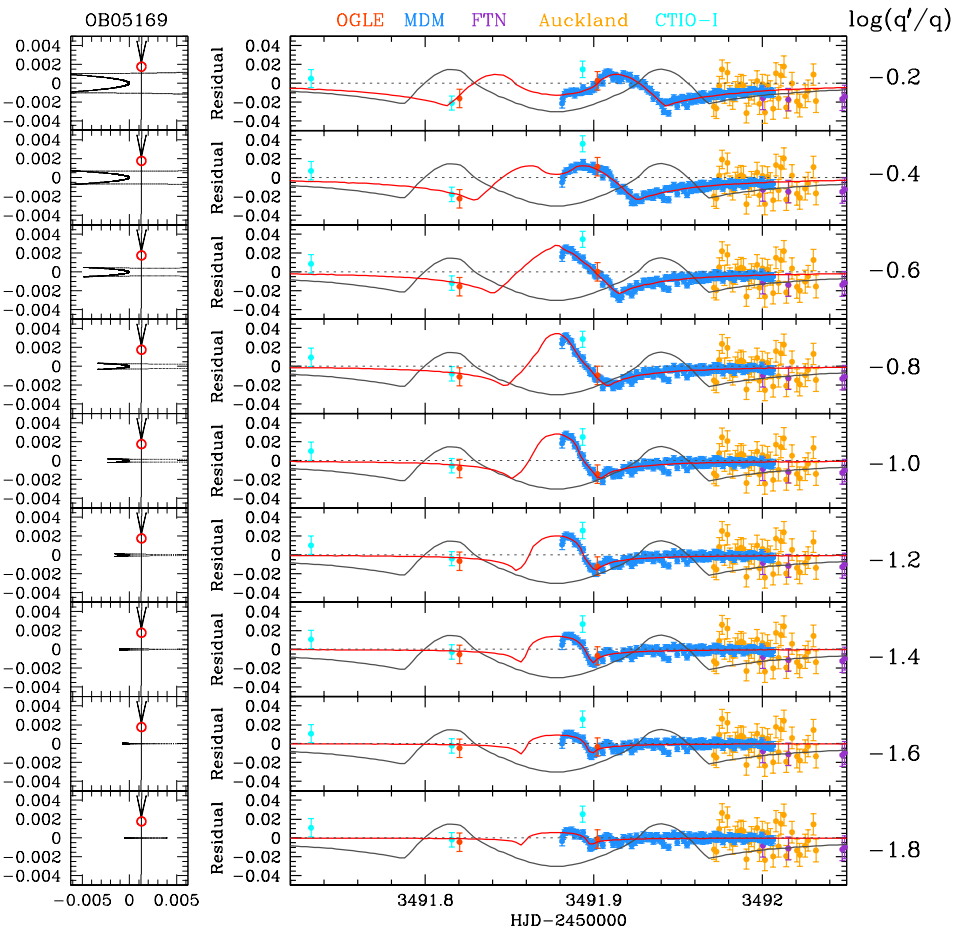

Fig. 13. Nine simulations of OGLE-2005-BLG-169, similar to Fig. 4. It is based on re-reduced data from all observatories, since these reductions would have been carried out whether or not a planet was suspected.

ily because of concerns that the quite small amplitude of the deviations might be due to variable weather conditions, which were very severe during the night of the anomaly. In the end, the decision to publish was based on the unambiguous discontinuous change of slope at HJD$'$ = 3491.97. Such discontinuities are a generic feature of microlensing caustic crossings but would be extremely difficult to produce by weather-induced artifacts.

Using the same criteria (and relying on the judgment of A.G., who made the original decision to publish) we conclude that the simulation with $\log(q'/q) = -1.2$ would marginally meet this condition. We fit simulated data at this value and find that $\sigma(\log q) = 0.174$, which does not satisfy our sample criterion. However, at $\log(q'/q) = -1.0$, we find $\sigma(\log q) = 0.10$, and so adopt $\log(q'/q) = -1.0$ as our threshold.

6.2. Constraints of the Mass-Ratio Function $F(q)$

If $F(q)$ is chosen correctly, then we expect the seven r_i defined by Eq.(10) to be uniformly distributed on the interval [0,1]. As discussed in the separate analyses of each event in Section 6.1 (and in particular, in subsection *OGLE-2013-BLG-0341*), in all cases P_i takes the form $P_i(q') = \Theta(10^{-4} - q)\Theta(q - q_{\min,i})$, where Θ is a Heaviside step function and $q_{\min,i}$ has been evaluated separately for each event. Hence Eq.(10) reduces to Eq.(11).

We expect then that

$$\frac{1}{N}\sum_{i=1}^{N} r_i = \frac{1}{2} \pm (12N)^{-1/2} \longrightarrow 0.500 \pm 0.109 \qquad (12)$$

where $N = 7$. We also expect that the distribution of r_i will be consistent with uniform based on a Kolmogorov-Smirnov (KS) test. To take an extreme example, if for a given trial function $F(q)$, each of the r_i were exactly equal to 0.58, then Eq.(12) would be satisfied, but the distribution would not be consistent with uniform $(p < 1\%)$. Nevertheless, since KS is a relatively weak test, it would be surprising if a function that satisfied Eq.(12) did not meet this second criterion as well.

We begin by considering power laws $F(q) \propto q^p$. Applying Eq.(12) we find that

$$p = 1.05^{+0.78}_{-0.68} \qquad \text{(this work)}. \qquad (13)$$

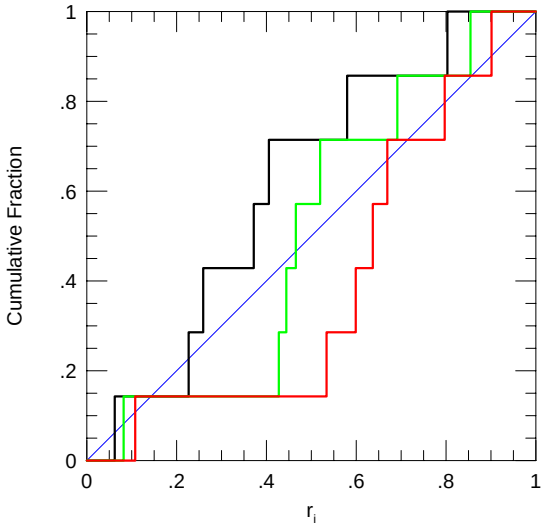

Fig. 14. Cumulative distribution of the "$V/V_{\max}$" parameter r_i defined by Eqs.(10) and (11) for three power laws $\mathrm{d}N/\mathrm{d}\ln q \propto q^p$, where q is the mass ratio and $p = 1.05$ (green), $p = 0.37$ (black), and $p = 1.83$ (red). These represent the best fit and 1σ lower and upper limits, respectively. In all cases, a Kolmogorov-Smirnov test shows that these are consistent with being drawn from a uniform distribution. Hence, there is no basis to reject a power-law for the mass-ratio function from this analysis. The best fit value confirms a sharp turnover in the mass-ratio function relative to that found by Sumi *et al.* (2010) and Suzuki *et al.* (2016) at higher mass ratios.

Fig. 14 shows the cumulative distribution at the best fit and 1σ limits displayed in Eq.(13). These have maximal differences (relative to uniform) of $D = (0.285, 0.309, 0.391)$ with corresponding KS p-values $p = (0.53, 0.43, 0.18)$. That is, there is no independent information from the uniformity (or lack of it) that would indicate that any of these functions is unacceptable at the 1σ level. Therefore, there is also no basis for rejecting a power-law form for the distribution in the domain probed by our sample.

Fig. 15 illustrates the "$V/V_{\rm max}$" method as well as the best fit result. For each event (listed at the top), the observed mass ratio q is shown by a blue point, while the lowest q' at which it could have been detected is shown by the bottom of the rectangular box. The boxes themselves have uniform width, which illustrates the relative frequency of q' values for the hypothetical case $\mathrm{d}N/\mathrm{d}\ln q \propto q^0 = \mathrm{const}$, *i.e.*, $p = 0$. The red curves show the relative frequency for the best-fit case, $p = 1.05$. The parameter r_i is the ratio of the volume "V" (*i.e.*, area) contained within the red curve above the actual detection, divided by the total volume "$V_{\rm max}$" within the red curve. The best-fit value ($p = 1.05$), illustrated in Fig. 15, occurs when $\langle r_i \rangle = 0.5$.

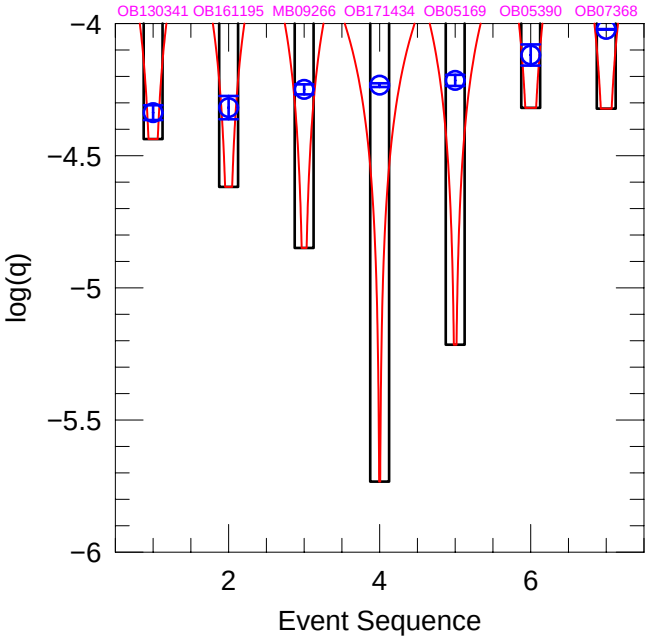

Fig. 15. Illustration of the "$V/V_{\rm max}$" method. The blue circles show the best fit q from the actual event, while the bottoms of the black rectangles show the lowest q' that could have been detected. The red curves show the relative frequency of different mass ratios according to the best-fit power law, $\mathrm{d}N/\mathrm{d}\ln q \propto q^{1.05}$. These can be compared to the relative frequencies that would be expected from a hypothetical law $\mathrm{d}N/\mathrm{d}\ln q = \mathrm{const}$ (black). If the frequency function is chosen correctly, then on average, half of the red "volume" should be above the blue points. More generally, the ratio r_i of this "volume" to the total "volume" should be consistent with being uniformly distributed over the interval [0,1].

Eq.(13) is consistent with the results of Suzuki *et al.* (2016), who found $p = 0.6^{+0.5}_{-0.4}$ based on an almost completely independent argument. Since these arguments are essentially independent, we can combine the two measurements (weighted according to the quoted errors) to obtain

$$p = 0.73^{+0.42}_{-0.34} \qquad (\text{this work} + \text{Suzuki } \textit{et al}.\ 2016). \tag{14}$$

The $V/V_{\rm max}$ statistical test presented here implicitly rests on the assumption that we (the authors) can determine "exactly" which planetary events are "publishable", or more precisely, "would have been published". This is clearly not the case. However, we estimate the typical error in our threshold determinations as $\sigma \approx 0.1$ dex, in the sense that at $2\sigma \approx 0.2$ dex higher, the planet would have very clearly been publishable and at $2\sigma \approx 0.2$ dex lower, it very clearly would not have been. We find that this level of variation in estimates leads to an additional uncertainty in the power law of 0.12. Because this is factor ≈ 6 smaller than the statistical error (Eq. 13) we are justified in ignoring it.

6.3. $\Delta\chi^2$ at Threshold

In contrast to the present investigation, all previous microlensing studies of the planet mass or mass-ratio function have used a detection-efficiency analysis, which compares the detected planets to a calculation of the overall planet sensitivity of the sample. The vast majority of these analyses calculate the planet sensitivity either by fitting planetary models to the data following Gaudi and Sackett (2000) or by simulating light curves with planets following Rhie *et al.* (2000). In both cases, the "detectability" of a given planet is assessed relative to a fixed $\Delta\chi^2$ threshold comparing 1L1S models to 2L1S[6]. Early analyses used $\Delta\chi^2 = 60$ as their detection threshold (Albrow *et al.* 2001, Gaudi *et al.* 2002), but other studies have used thresholds ranging from $\Delta\chi^2 = 60$ to $\Delta\chi^2 = 500$ (Sumi *et al.* 2010, Gould *et al.* 2010, Cassan *et al.* 2012, Suzuki *et al.* 2016). In the analysis of individual events, different authors have used different thresholds depending on the exact event and on whether or not the planet signal comes from a central caustic or a planetary caustic (*e.g.*, Section 8 of Sumi *et al.* 2010 and references therein). For example, Yee *et al.* (2013) argued based on the analysis of MOA-2010-BLG-311 that $\Delta\chi^2 \approx 80$ is insufficient to claim a secure planet detection, even though this is above the $\Delta\chi^2$ threshold used in many studies. They also suggested that this event is evidence that the threshold for high-magnification/central-caustic crossing perturbations may be higher than for planetary caustic perturbations.

Although the $V/V_{\rm max}$ analysis presented here was designed to answer a different question, we can use the results of this analysis to explore $\Delta\chi^2$ at the threshold of planet detection. Table 3 shows $\Delta\chi^2 \equiv \chi^2(\text{1L1S}) - \chi^2(\text{2L1S})$ [or $\chi^2(\text{2L1S}) -$

[6]The exception is Shvartzvald *et al.* (2016), who used a local χ^2 excess to determine detectability with the threshold determined individually for each event.

Table 3

$\Delta\chi^2$

Event	$(\log q'/q)$	χ^2(2L1S)	χ^2(1L1S)	$\Delta\chi^2$
OB05169	-1.0	506	690	184
OB161195	-0.3	12415	12672	257
OB130341	-0.1	8874	9183	309
OB05390	-0.2	551	1008	457
OB07368	-0.3	2625	3326	701
OB170173 (A)	-0.7	7435	8389	954
OB170173 (B)	-0.7	7432	8582	1150
MB09266	-0.6	4153	24497	20344
OB171434	-1.5	18236	22247	4011

$\chi^2(3\mathrm{L1S})$ in the case of OGLE-2013-BLG-0341] at our adopted threshold of "publishability" for the eight events considered here (including two models for OGLE-2017-BLG-0173). The most striking feature of Table 3 is that $\Delta\chi^2$ at threshold spans a factor of 100. As we discuss below, the extreme broadness of this range is partly due to the heterogeneous character of the sample. However, even after accounting for this heterogeneity, Table 3 strongly suggests that $\Delta\chi^2$ is a relatively poor proxy for "publishability". Before we begin this review, we emphasize that we regard "publishability" as a more appropriate criterion that "detectability" because anomalies can be "detectable" and unambiguously real, yet still be uninterpretable at a level that is scientifically interesting.

The four events for which the threshold was $\Delta\chi^2 < 500$ shed the most light on this question: OGLE-2005-BLG-169, OGLE-2016-BLG-1195, OGLE-2013-BLG-0341, and OGLE-2005-BLG-390, with $\Delta\chi^2 = 184$, 257, 309, and 457, respectively. These are naturally grouped into two pairs: OGLE-2005-BLG-169 and OGLE-2013-BLG-0341 were both identified from very short features whose signatures were unambiguously planetary, while for both OGLE-2016-BLG-1195 and OGLE-2005-BLG-390, the threshold was set by confusion with 1L2S models.

As discussed in Section 6.1 (*OGLE-2005-BLG-169*), the actual decision to publish OGLE-2005-BLG-169 was based on the secure recognition of a discontinuity in the slope of the light curve. Such discontinuities cannot be produced by any microlensing effect other than a planetary (or binary) companion and would be extremely difficult to generate by instrumental or weather problems. We found in Section 6.1 (*OGLE-2005-BLG-169*) that at the threshold of "by-eye confidence" in the reality of this feature, the mass-ratio error $\sigma(\log q) = 0.10$ is relatively close to our adopted threshold of $\sigma(\log q) < 0.15$. Thus, by two independent modes of assessment, this event would have been "barely publishable" at the adopted threshold.

For OGLE-2013-BLG-0341, the key signature was an isolated dip, which can only be produced by a minor-image perturbation. Moreover, such short-lived dips

can only be produced by planets. While the total $\Delta\chi^2$ of the planet is higher than that of OGLE-2005-BLG-169 by 125, this difference is somewhat deceptive. Recall from Section 6.1 (*OGLE-2013-BLG-0341*) that $\Delta\chi^2(\text{binary-caustic}) = 66$ came from the perturbation induced by the binary caustic. However, this binary-caustic "confirmation" played no role in our assessment of whether the planet would have been published at the adopted threshold. Hence, if the system had been a simple 2L1S system, or if the trajectory happened to miss the central caustic, the decision would have been exactly the same. In these cases, $\Delta\chi^2 = 309 - 66 = 243$. Moreover, we have not attempted to assess the exact $\log q'/q$ at which the event would have ceased to be publishable, mainly because this level of precision would not contribute significantly to our study, but also because we do not believe that such precision is feasible. Hence, these two values (184 and 243) for these two "short timescale feature" events should be regarded as comparable.

In brief, based on this admittedly small sample of two, it appears feasible to publish "short timescale feature" events with $\Delta\chi^2 \gtrsim 200$.

It is quite notable that the two events whose threshold is set by confusion with 1L2S models have substantially different $\Delta\chi^2$ in Table 3, *i.e.*, 257 *vs.* 457. It is true OGLE-2005-BLG-390 was subjected to a slightly stronger $\Delta\chi^2$ threshold to reject 1L2S ($\Delta\chi^2 > 16$ *vs.* 12), which drove up its threshold of acceptance from $\log(q'/q) = -0.25$ to $\log(q'/q) = -0.20$. However, it is also the case that at the finally adopted threshold for OGLE-2013-BLG-1195, it met essentially the same threshold (see Section 6.1, *OGLE-2016-BLG-1195*). Hence, this is not a major factor in this difference. Furthermore, at their respective thresholds, which differ in $\Delta\chi^2$ by a factor 1.8, both events have very similar $\sigma(\log q) \simeq 0.1$. Hence, based on this very small sample of two "1L2S-limited" events, we already see a very significant difference in $\Delta\chi^2$ at threshold.

The remaining four events have larger $\Delta\chi^2$ between the 1L1S and 2L1S solutions at the threshold. However, because of their more complex observation history, interpreting their significance for understanding $\Delta\chi^2$ thresholds in general would require significantly more investigation than provided by the $V/V_{\rm max}$ analysis. Nevertheless, we review here what is known from the present analysis.

For OGLE-2008-BLG-0368, the $\Delta\chi^2 = 701$ appears substantially larger than the previous four cases, particularly because it contains a short-duration "dip", which we noted above is a signature of a minor image perturbation that is very difficult to mimic by other (non-planetary) effects. Recall from Section 6.1 (*OGLE-2007-BLG-368*), however, that the threshold was set by the availability of follow-up data. Therefore, while we do not investigate this issue in detail, we can be confident that the $\Delta\chi^2$ threshold for a similar event with data acquisition that did not depend on alerts (*i.e.*, without triggered, follow-up data), would be significantly smaller. That is, this event does not, in itself, provide evidence for a substantially broader range of $\Delta\chi^2$ threshold than has already been established above.

The two variants of OGLE-2017-BLG-0173 both have $\Delta\chi^2 \approx 1000$, which is again relatively high compared to the four lowest-$\Delta\chi^2$ events. This high $\Delta\chi^2$ results directly from our assessment that a bump with amplitude $\Delta I \lesssim 0.06$ mag would not have been noticed in the current mode of KMTNet review of OGLE-discovered events. However, this bump was very densely covered from two KMTNet observatories. We hypothesize that a future, systematic, algorithm-based search for anomalies (rather than the by-eye search) would likely have discovered such a bump even at substantially lower amplitude. Although "potential" (*i.e.*, future) discoveries are irrelevant to the $V/V_{\rm max}$ analysis, they are relevant to the question of establishing an appropriate $\Delta\chi^2$ threshold. The enhanced sensitivity of such searches would easily bring the threshold for this event into the $\Delta\chi^2$ range of events like OGLE-2005-BLG-390. Hence, in the context of a future, machine search for anomalies, the present analysis provides only an upper limit for the $\Delta\chi^2$ threshold.

The case of OGLE-2017-BLG-1434, with $\Delta\chi^2 = 4011$, is even more stark. Part of the issue here is that for purposes of the current study, we were forced to consider "quick look" data, which were reduced for only one of the two KMTNet fields, while the reported $\Delta\chi^2$ value is based on data from both fields. Hence, from the standpoint of studying thresholds, we should really consider that this event has $\Delta\chi^2 = 2005$. Even so, this is quite high relative to the first four events that we examined above. Recall from Section 6.1 (*OGLE-2017-BLG-1434*), that we rejected $\log(q'/q) = -1.75$ because, within the context of the visual reviews by which planets are currently being discovered in KMTNet data, this would have appeared to have had a single strong outlier, with a few other deviating points that could easily be taken for noise. A machine search would easily identify the planetary anomaly at $\log(q'/q) = -1.75$ in the data shown in Fig. 4, and this would have then led to publication, even if only data from one KMTNet field were available. Thus, as with OGLE-2017-BLG-0173, the $\Delta\chi^2$ threshold for a more homogeneous search would be much lower than in the current study, which provides only an upper limit on the threshold.

Finally, the very high $\Delta\chi^2 = 20345$ for MOA-2009-BLG-266 is an order of magnitude larger than for any other events considered here. A major factor is that, as discussed in Section 6.1, (*MOA-2009-BLG-266*), the threshold is set by the requirement of an alert, which then greatly increased the $\Delta\chi^2$ at the threshold. Further investigation and assessment of the influence of follow-up data on the $\Delta\chi^2$ threshold in this potentially interesting case is outside the scope of the present study.

The $\Delta\chi^2$ values from Table 3 provide an interesting window into the role of $\Delta\chi^2$ as a proxy for publishability. However, because the current study is founded on an inhomogeneous sample of planetary events, this review of these $\Delta\chi^2$ cannot be regarded as a definitive investigation of this question. In our view, the review provides evidence that the $\Delta\chi^2$ threshold for homogeneous samples is likely to vary at the factor 2 level but a more focused study would be required to confirm this.

6.4. Host Mass of Low-q Planets

Fig. 16 shows the planet-host mass ratio q *vs.* host mass M for the eight planets with low mass ratios: $q < 10^{-4}$. Microlenses with well measured host masses (either from parallax or direct imaging) are shown in black, while those with Bayesian estimates are shown in red. The two green points show the ambiguous q determination for OGLE-2017-BLG-0173, which is excluded from the present study because of this ambiguity, but is displayed here for completeness[7].

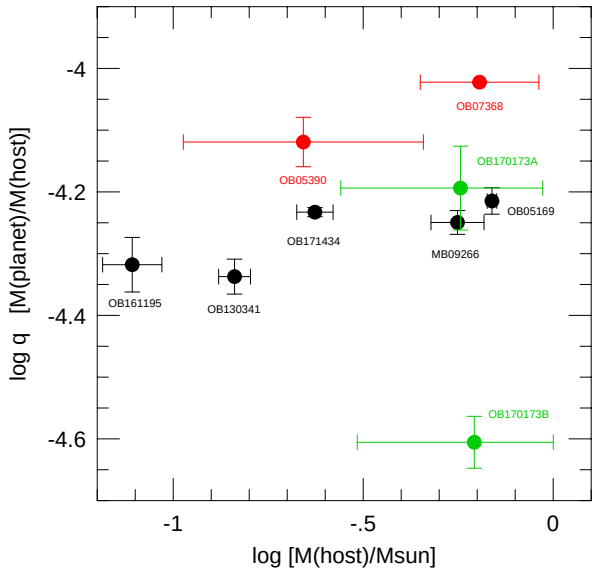

Fig. 16. Mass ratio q *vs.* host mass M for eight microlensing planets with best-fit mass ratios $q < 10^{-4}$. The black points have well-measured host masses, either from microlens parallax or direct imaging (left to right, OGLE-2016-BLG-1195, OGLE-2013-BLG-0341, OGLE-2017-BLG-1434, MOA-2009-BLG-266, and OGLE-2005-BLG-169). The red points have host masses derived from Bayesian estimates (OGLE-2005-BLG-390 and OGLE-2007-BLG-368). The green points show two different degenerate models for OGLE-2017-BLG-0173, which is not included in our statistical sample. The range of host masses is one dex while the range of mass ratios is one octave, suggesting that planet-host mass ratio is a better defined function than planet mass.

The main implication of Fig. 16 is that the range in $\log M$ is about three times larger than in $\log q$. The broad range in $\log M$ is not the result of measurement

[7]The host masses for the two solutions of OGLE-2017-BLG-0173 are corrected relative to those given by Hwang *et al.* (2018), which were impacted by a bug in the Bayesian code. In particular, the median of the correct estimates of the mass are about 1.5 times higher than the original estimates. These corrections have no impact on the present study, in part because it deals with mass ratios (which are unaffected) rather than masses, but also because OGLE-2017-BLG-0173 is excluded from the study. However, it does impact the host mass shown in Fig. 16. For completeness, we report here the corrected Bayesian estimates for models (A,B,C): $M_{\rm host} = (0.57^{+0.38}_{-0.29}, 0.62^{+0.38}_{-0.32}, 0.62^{+0.37}_{-0.31})$ $M_\odot$, $M_{\rm planet} = (12^{+11}_{-7}, 5.1^{+5.1}_{-2.8}, 14^{+11}_{-8})$ $M_\oplus$, $D_{\rm L} = (5.9^{+1.0}_{-1.5}, 5.5^{+1.1}_{-1.5}, 5.6^{+1.0}_{-1.5})$ kpc, $a_\perp = (4.3^{+1.2}_{-1.3}, 4.6^{+1.3}_{-1.5}, 4.4^{+1.2}_{-1.4})$ a.u.

errors: it would remain the same even if the two red points were excluded. In this section, we have shown (see Fig. 15) that the restricted range in $\log q$ is not a selection effect. That is, many (though not all) of these planets could have been detected at much lower q. Fig. 16 suggests, although it certainly does not prove, that the planet mass-ratio function is a better framework for understanding planet masses than the planet mass function. That is, it suggests that the turnover first pointed out by Suzuki *et al.* (2016), and confirmed in this section, is a turnover in planet mass ratio rather than in planet mass.

In this context, it is interesting to note that in a study carried out contemporaneously with the present one, Pascucci *et al.* (2018) found that the mass-ratio function derived from Kepler planets with periods $P < 100$ d is independent of host mass for hosts $M < 1$ M$_\odot$. They found a broken power law, with a slope at the low-mass end that is consistent with those derived here and by Suzuki *et al.* (2016), but with the break roughly a decade below the one found by Suzuki *et al.* (2016). In brief, there is some evidence from the present study that planet-host mass ratio governs planet formation outside the snow line and stronger evidence from Pascucci *et al.* (2018) that this is the case inside the snow line, even though planet formation peaks at very different mass ratios in these two zones.

Finally, we note that one of the solutions for OGLE-2017-BLG-0173 (blue points) has similar q to those of the seven other points, while the other is separated from the entire group by almost 0.3 dex. While no strong conclusion can be drawn from this, it suggests that the higher mass-ratio solution is correct. Unfortunately, as discussed by Hwang *et al.* (2018), it is quite unlikely that this degeneracy will be resolved by future follow-up observations.

7. Conclusions

With a planet-host mass ratio $q = 5.8 \times 10^{-5}$ and planet mass $m_p = 4.4 M_\oplus$, OGLE-2017-BLG-1434Lb facilitates a new probe of cold, low-mass planets. It is the eighth microlensing planet with $q < 10^{-4}$. Combining seven of these detections, and applying a new "$V/V_{\rm max}$" argument, we have shown that the planet-host mass-ratio function turns over at low mass. That is, it rises sharply toward lower mass for $q \gtrsim 2 \times 10^{-4}$ (power law $n \approx -1$) but then falls just as sharply toward lower mass for $q < 10^{-4}$ (power law $p \approx +1$).

Acknowledgements. We thank the anonymous referee for useful remarks. Work by WZ, YKJ, and AG were supported by AST-1516842 from the US NSF. WZ, IGS, and AG were supported by JPL grant 1500811. Work by C.H. was supported by the grant (2017R1A4A1015178) of National Research Foundation of Korea. This research has made use of the KMTNet system operated by the Korea Astronomy and Space Science Institute (KASI) and the data were obtained at three host sites of CTIO in Chile, SAAO in South Africa, and SSO in Australia.

The OGLE project has received funding from the National Science Centre, Poland, grant MAESTRO 2014/14/A/ST9/00121 to AU. Work by YS was supported by an appointment to the NASA Postdoctoral Program at the Jet Propulsion Laboratory, California Institute of Technology, administered by Universities Space Research Association through a contract with NASA.

REFERENCES

Alard, C., and Lupton, R.H. 1998, *ApJ*, **503**, 325.
Albrow, M.D., *et al.* 2001, *ApJ*, **556**, L113.
Albrow, M.D., *et al.* 2009, *MNRAS*, **397**, 2099.
Batista, V., *et al.* 2011, *A&A*, **529**, 102.
Batista, V., Beaulieu, J.-P., Bennett, D.P., Gould, A., Marquette, J.-B., Fukui, A., and Bhattacharya, A. 2015, *ApJ*, **808**, 170.
Beaulieu, J.-P. *et al.* 2006, *Nature*, **439**, 437.
Bennett, D.P., *et al.* 2008, *ApJ*, **684**, P663.
Bennett, D.P., *et al.* 2015, *ApJ*, **808**, 169.
Bensby, T., *et al.* 2013, *A&A*, **549A**, 147.
Bessell, M.S., and Brett, J.M. 1988, *PASP*, **100**, 1134.
Bond, I.A., *et al.* 2017, *MNRAS*, **469**, 2434.
Bramich, D.M. 2008, *MNRAS*, **386**, L77.
Calchi Novati, S., *et al.* 2015, *ApJ*, **804**, 20.
Cassan, A., *et al.* 2012, *Nature*, **481**, 167.
Dominik, M., *et al.* 2007, *MNRAS*, **380**, 792.
Evans, D.F., *et al.* 2016, *A&A*, **589**, 58.
Gaudi, B.S. 2012, *Ann. Rev. Astron. Astrophys.*, **50**, 411.
Gaudi, B.S., and Sackett, P. 2000, *ApJ*, **528**, 56.
Gaudi, B.S., *et al.* 2002, *ApJ*, **566**, 463.
Gould, A. 1992, *ApJ*, **392**, 442.
Gould, A. 1997, in: "Variables Stars and the Astrophysical Returns of the Microlensing Surveys". Eds. R. Ferlet, J.-P. Maillard and B. Raban. Gif-sur-Yvette, France : Editions Frontieres, p.125.
Gould, A. 2000, *ApJ*, **542**, 785.
Gould, A. 2004, *ApJ*, **606**, 319.
Gould, A. 2008, *ApJ*, **681**, 1593.
Gould, A., and Andronov, N. 1999, *ApJ*, **516**, 236.
Gould, A., *et al.* 2006, *ApJ*, **644**, L37.
Gould, A., *et al.* 2010, *ApJ*, **720**, 1073.
Gould, A., and Horne, K. 2013, *ApJ*, **779**, L28.
Gould, A., *et al.* 2014, *Science*, **345**, 46.
Gould, A., Yee, J., and Carey, S. 2015a, Spitzer Proposal 12013.
Gould, A., Yee, J., and Carey, S. 2015b, Spitzer Proposal 12015.
Han, C. 2006, *ApJ*, **638**, 1080.
Han, C., *et al.* 2016, *ApJ*, **827**, 11.
Hwang, K.-H., *et al.* 2018, *AJ*, **155**, 20.
Kayser, R., Refsdal, S., and Stabell, R. 1986, *A&A*, **166**, 36.
Kennedy, G.M., and Kenyon, S.J. 2008, *ApJ*, **673**, 502.
Kervella, P., Thévenin, F., Di Folco, E., and Ségransan, D. 2004, *A&A*, **426**, 297.
Kim, S.-L., *et al.* 2016, *Journal of the Korean Astronomical Society*, **49**, 37.
Kubas, D., *et al.* 2012, *A&A*, **540A**, 78.

Mróz, P., *et al.* 2017, *AJ*, **153**, 143.
Muraki, Y., *et al.* 2011, *ApJ*, **741**, 22.
Nataf, D.M., *et al.* 2013, *ApJ*, **769**, 88.
Pascucci, I., Mulders, G.D., Gould, A., and Fernandes, R. 2018, *ApJ*, **856**, 28.
Paczyński, B. 1986, *ApJ*, **304**, 1.
Pejcha, O., and Heyrovský, D. 2009, *ApJ*, **690**, 1772.
Rhie, S.H., *et al.* 2000, *ApJ*, **533**, 378.
Ryu, Y.-H., *et al.* 2017, *AJ*, **154**, 247.
Schmidt, M. 1968, *ApJ*, **151**, 393.
Schneider, P., and Weiss, A. 1988, *ApJ*, **330**, 1.
Shvartzvald, Y., *et al.* 2016, *MNRAS*, **457**, 4089.
Shvartzvald, Y., *et al.* 2017, *ApJ*, **840**, L3.
Skottfelt, J., *et al.* 2015, *A&A*, **574**, 54.
Skowron, J., *et al.* 2011, *ApJ*, **738**, 87.
Spergel, D.N., *et al.* 2013, arXiv:1305.5422.
Sumi, T., *et al.* 2010, *ApJ*, **710**, 164.1
Suzuki, D., *et al.* 2016, *ApJ*, **833**, 145.
Udalski, A. 2003, *Acta Astron.*, **53**, 291.
Udalski, A., Szymański, M., Kaluzny, J., Kubiak, M., Mateo, M., Krzeminski, W., and Paczyński, B. 1994, *Acta Astron.*, **44**, 227.
Udalski, A., Szymański, M.K., and Szymański, G. 2015, *Acta Astron.*, **65**, 1.
Wambsganss, J. 1997, *MNRAS*, **284**, 172.
Woźniak, P.R. 2000, *Acta Astron.*, **50**, 421.
Yee, J.C., *et al.* 2012, *ApJ*, **755**, 102.
Yee, J.C., *et al.* 2013, *ApJ*, **769**, 77.
Yee, J.C., *et al.* 2015, *ApJ*, **810**, 155.
Zhu, W., *et al.* 2017, *AJ*, **154**, 210.